periodic boundary box of 100 Å × 100 Å × 250 Å in which the top and bottom parts of HA were set apart from the boundary by more than 10 Å (Figure 1c). Consequently, the total number of atoms was about 259,300 in each model.

MD simulations were carried out for every model using NAMD ver. 2.6.[42] Initially, energy minimization was executed for 1,000,000 steps with the conjugate gradient method. Next, the temperature of the model system was elevated up to 310 K. Then 30 ns equilibrating simulation was performed in the NTP ensemble condition to obtain the equilibrated structures of the wild-type HA and the three kinds of mutants. Nonbonded interaction terms were computed with a cutoff distance of 12 Å, where a switching distance of 10 Å was applied to make the nonbonded interaction zero at the cutoff distance smoothly. A periodic boundary condition was applied to all directions of the calculation cell, and the particle mesh Ewald method was employed to compute the long-distance nonbonded interaction. CHARMM27 force field[43] was adopted for all atoms.

Docking Simulation. The binding modes of stachyflin to the wild-type HA and its mutants were predicted by docking simulation using GOLD ver. 4.[44,45] The equilibrated structure obtained from the MD simulation was utilized as a plausible protein structure of HA in the wild-type and three mutants. Binding score was also calculated to evaluate the difference in binding affinity due to the mutations. A preliminary docking calculation was executed to search for the docking area within 30 Å from Phe110 of the HA2 subunit. Since an adequate docking space was found inside the area and stachyflin was positioned near Asp109 in the binding mode ranking first, recalculation of stachyflin docking was performed with the search area set within 10 Å from Asp109 of HA2 subunit. Fifty binding poses were generated and the binding affinities of those binding poses were estimated by GOLD score function. On the basis of the ranking in the estimated GOLD score, the most probable binding pose was selected. The binding affinity for the selected binding pose was re-estimated using ASP score function. This two-step approach, *i.e.*, determination of the binding pose with GOLD score and subsequent estimation of binding affinity with ASP score, was reported to successfully provide reliable prediction in docking of low-molecular-weight ligands to an enzyme or receptor.[46,47]

***In Silico* Screening.** A search for compounds bearing chemical features similar to those of stachyflin was made by an *in silico* pharmacophore screening. A chemical database was provided by Namiki Co. Ltd., in which about 3 million synthesized compounds are listed and all of the compounds are available by purchase. First, conformations of every compound were generated by using OMEGA module of OpenEye software.[48] Totally, more than 200 million chemical conformations were generated. Second, the pharmacophore of stachyflin was extracted for setting queries, in which hydrogen-bond donor and acceptor, aromatic ring, and hydrophobic region appeared to be key features. Third, chemical screening was carried out from the viewpoint of structural similarity to stachyflin using ROCS module of OpenEye.[49] A total of 5094 compounds were extracted from the Namiki database under the condition of the Tanimoto coefficient being more than 0.75. Fourth, more condensed selection of chemicals from the 5094 compounds was performed using EON module[49] from the viewpoint of similarity in charge distribution. The compounds without structural flexibility were excluded. Consequently, 8 chemical compounds were selected as candidates for purchase.

Synthesis of Analogue Compounds. Two series of derivatives were synthesized in this work. One is an analogue containing a vanillic acid skeleton, and the other is one bearing thieno-pyrimidine. Compound **9**, 3-methoxy-4-[(methyl-sulfonyl)oxy]-benzoic acid methoxy-ester, is a typical derivative of the former series. A mixture of vanillic acid methyl (1.0 g, 5.49 mmol), KCO_3 (1.13 g, 8.24 mmol), and acetonitrile (30 mL) was cooled in an ice bath under Ar atmosphere. Methane-sulfonyl chloride (0.51 mL, 6.59 mmol) was slowly added to the mixture, and then the solution was mechanically stirred for 3 h at RT. The reaction mixture was filtered with Celite, and the solvent was removed *in vacuo*. The resulting product was extracted with a solution of EtOAc (30 mL) and 1 M aqueous HCl (30 mL). The aqueous layer was treated with EtOAc (20 mL) two times, and the combined organic layer was washed with brine, dried over $MgSO_4$, and concentrated *in vacuo*. The product was purified by thin-layer chromatography with hexane/EtOAc in a ratio of 3:1. The solid obtained was resuspended with a solution of hexane and EtOAc, and recrystallization produced the final compound as a white solid (1.01 g, yield 71%).

A typical derivative of the latter series is compound **35**, 4-(4-methyl-1-pyperazinyl)-thieno[2,3-*d*]pyrimidine hydrochloride salt. 4-Chloro-thieno[2,3-*d*]pyrimidine (200 mg, 1.17 mmol) was solvated with THF (15 mL). After addition of 1-methyl-pyperazine (0.26 mL, 2.34 mmol) and NaOH (0.94 g, 2.34 mmol), the mixture was heated under reflux for 6 h. The solvent was removed *in vacuo*, and the reaction mixture was treated with a solution of EtOAc (20 mL) and distilled H_2O (15 mL). The product was extracted with EtOAc two times, and the organic layer was washed with brine and dried over Na_2SO_4. The solvent was evaporated *in vacuo*, and the resulting product was purified by two-dimensional thin-layer chromatography with hexane/EtOAc in ratios of 3:1 and 1:1. A brown solid of (phenyl pyperazinyl)-theino-pyrimidine was obtained in a yield of 54% (148 mg). The solid obtained was resuspended in a solution of toluene (20 mL) and 1 M aqueous HCl (0.6 mL) and heated under reflux for 1 h. The reaction solution was cooled to RT, and filtration gave the final compound as a brownish solid (127 mg, yield 45%).

Antiviral Assay. Compound potency was tested by an influenza virus cell culture assay with measurement of the quantity of viral RNA using real-time polymerase chain reaction (RT-PCR). Test compounds were mixed with minimum essential medium (MEM) containing bovine serum albumin (BSA). To prepare a virus-containing compound-mixed medium, 100 units of 50% tissue culture infective dose (TCID50) of influenza virus A/Perto Rico/8/34 strain (PR8) was suspended in 100 μL of the MEM-BSA containing test compounds and 10 μg/mL of acetylated trypsin. Madin-Darby canine kidney (MDCK) cells were loaded in a 96-well plate. The cells were washed with phosphate-buffered saline (PBS), followed by 0.5−1 h incubation with compound-mixed medium. The virus-containing compound-mixed medium was also incubated for 0.5−1 h. After incubation, MDCK cells in the compound-mixed medium without viruses were transferred to the compound-mixed medium with viruses. Then the cells were incubated for 1 h at 37 °C in 100 μL of the virus-containing compound-mixed medium (100 TCID50 influenza virus, 10 μg/mL acetylated trypsin, and test compound at several concentrations). MDCK cells were washed with compound-mixed medium without viruses and incubated in the compound-mixed, acetylated trypsin-containing medium without influenza virus for 24 h. Culture supernatants of MDCK cells were collected after the incubation, and RNA was extracted from the supernatants. The amount of viral RNA was measured by the RT-PCR method. The measurement was compared to that of the control that was performed in a similar manner without any test compound. The compound concentration to suppress viral proliferation to 50% (EC_{50}) was estimated from the comparison.

RNA Extraction and RT-PCR. To monitor the efficiency of RNA purification, uninfected VeroE6 cells were mixed in the ISOGEN reagent as a source of 18S rRNA for normalization. Supernatants from MDCK cell culture medium were mixed with ISOGEN reagent and RNA was purified according to the manufacturer's protocol. For quantification of PR8 HA RNA, real-time RT-PCR was performed using the primers and the probe with the sequences of PR8-HA-F: 5′-GGCAAATGGAAATCTAATAGCACC-3′, PR8-HA-R: 5′-TGATGCTTTTGAGGTGATGA-3′, and PR8-HA-probe: 5′-FAM-TCGCACTGAGTAGAGGCTTTGGGTCC-TAMRA-3′. For monitoring efficiency of RNA purification, 18S rRNA was quantified using the primers and the probe with the sequences of 18S-F: 5′-GTAACCCGTTGAACCCCATT-3′, 18S-R: 5′-CCATCCAATCGG-TAGTAGCG-3′, and 18S-probe: 5′-FAM-TGCGTTGAT-TAAGTCCCTGCCCTTTGTA-TAMRA-3′. The intensity of fluorescence emitted from the probe was detected by the ABI-7700 sequence detector system (Applied Biosystems).

ASSOCIATED CONTENT

Supporting Information

Composition of lipid membrane models, predicted binding affinities, RMSDs during MD simulation, predicted binding structures of stachyflin, superimposition of HA structures, chemical properties of synthesized compounds, and their NMR spectra. This material is available free of charge *via* the Internet at http://pubs.acs.org.

AUTHOR INFORMATION

Corresponding Author

*E-mail: (N.Y.) n-yama-5@nih.go.jp; (T.H.) hoshino@chiba-u.jp.

Author Contributions

#These authors contributed equally to this work.

ACKNOWLEDGMENTS

We thank L.Q. Mai (National Institute of Hygiene and Epidemiology, Hanoi) for providing the A/Vietnam/1194/04 virus strain. This work was partly supported by a Health and Labor Science Research Grant for Research from the Ministry of Health and Labor of Japan. This work was also supported by a Grant-in-Aid for Scientific Research (C) from Japan Society for the Promotion of Science (JSPS). This study was also supported in part by a grant-in-aid (S0991013) from the Ministry of Education, Culture, Sport, Science, and Technology, Japan (MEXT) for the Foundation of Strategic Research Projects in Private Universities. Theoretical calculations were performed at the Research Center for Computational Science, Okazaki, Japan and at the Information Technology Center of the University of Tokyo and also by the high-performance computer system at Institute for Media Information Technology in Chiba University.

REFERENCES

(1) Gambotto, A., Barratt-Boyes, S. M., de Jong, M. D., Neumann, G., and Kawaoka, Y. (2008) Human infection with highly pathogenic H5N1 influenza virus. *Lancet 371*, 1464−1475.

(2) Beigel, J. H., Farrar, J., Han, A. M., Hayden, F. G., Hyer, R., de Jong, M. D., Lochindarat, S., Nguyen, T. K. T., Nguyen, T. H., Tran, T. H., Nicoll, A., Touch, S., Yuen, K. Y., and Writing Committee of the World Health Organization Consultation on Human Influenza A/H5. (2005) Avian influenza A (H5N1) infection in humans. *N. Engl. J. Med. 353*, 1374−1385.

(3) Schnell, J. R., and Chou, J. J. (2008) Structure and mechanism of the M2 proton channel of influenza A virus. *Nature 451*, 591−595.

(4) Stouffer, A. L., Acharya, R., Salom, D., Levine, A. S., Di Costanzo, L., Soto, C. S., Tereshko, V., Nanda, V., Stayrook, S., and DeGrado, W. F. (2008) Structural basis for the function and inhibition of an influenza virus proton channel. *Nature 451*, 596−599.

(5) McNicholl, I. R., and McNicholl, J. J. (2001) Neuraminidase inhibitors: zanamivir and oseltamivir. *Ann. Pharmacother. 35*, 57−70.

(6) Moscona, A. (2005) Neuraminidase inhibitors for influenza. *N. Engl. J. Med. 353*, 1363−1373.

(7) Bright, R. A., Medina, M.-j., Xu, X., Perez-Oronoz, G., Wallis, T. R., Davis, X. M., Povinelli, L., Cox, N. J., and Klimov, A. I. (2005) Incidence of adamantane resistance among influenza A (H3N2) viruses isolated worldwide from 1994 to 2005: a cause for concern. *Lancet 366*, 1175−1181.

(8) Deyde, V. M., Xu, X., Bright, R. A., Shaw, M., Smith, C. B., Zhang, Y., Shu, Y., Gubareva, L. V., Cox, N. J., and Klimov, A. I. (2007) Surveillance of resistance to adamantanes among influenza A(H3N2) and A(H1N1) viruses isolated worldwide. *J. Infect. Dis. 196*, 249−257.

(9) Kitahori, Y., Imanishi, Y., and Inoue, Y. (2008) High incidence of amantadine-resistant influenza H1N1 viruses isolated during the 2007−2008 season in Nara Prefecture, Japan. *Jpn. J. Infect. Dis 61*, 253−254.

(10) Kamigauchi, T.; Fujiwara, T.; Tani, H.; Kawamura, Y.; Horibe, I. Shionogi & Co, Ltd. Sesquiterpene derivatives having antiviral activity, Patent WO/1997/011947, 1997.

(11) Taishi, T., Takechi, S., and Mori, S. (1998) First total synthesis of (±)-stachyflin. *Tetrahedron Lett. 39*, 4347−4350.

(12) Yoshimoto, J., Kakui, M., Iwasaki, H., Fujiwara, T., Sugimoto, H., and Hattori, N. (1999) Identification of a novel HA conformational change inhibitor of human influenza virus. *Arch. Virol. 144*, 865−878.

(13) Yoshimoto, J., Kakui, M., Iwasaki, H., Sugimoto, H., Fujiwara, T., and Hattori, N. (2000) Identification of amino acids of influenza virus HA responsible for resistance to a fusion inhibitor, Stachyflin. *Microbiol. Immunol. 44*, 677−685.

(14) Rosenbaum, D. M., Cherezov, V., Hanson, M. A., Rasmussen, S. G. F., Thian, F. S., Kobilka, T. S., Choi, H. J., Yao, H. J., Weis, W. I., Stevens, R. C., and Kobilka, B. K. (2007) GPRC engineering yields high-resolution structural insights into β2-adrenergic receptor function. *Science 318*, 1266−1273.

(15) Wegener, A. A., Klare, J. P., Engelhard, M., and Steinhoff, H. J. (2001) Structural insights into the early steps of receptor-transducer signal transfer in archaeal pototaxis. *EMBO J. 20*, 5312−5319.

(16) Sato, Y., Hata, M., Neya, S., and Hoshino, T. (2005) Computational analysis of the transient movement of helices in sensory rhodopsin II. *Protein Sci. 14*, 183−192.

(17) Cross, K. J., Burleigh, L. M., and Steinhauer, D. A. (2001) Mechanisms of cell entry by influenza virus. *Exp. Rev. Mol. Med. 3*, 1−15.

(18) Bodian, D. L., Yamasaki, R. B., Buswell, R. L., Stearns, J. F., White, J. M., and Kuntz, I. D. (1993) Inhibition of the fusion-inducing conformational change of influenza hemagglutinin by benzoquinones and hydroquinones. *Biochemistry 32*, 2967−2978.

(19) Luo, G., Colonno, R., and Krystal, M. (1996) Characterization of hemagglutinin-specific inhibitor of influenza A virus. *Virology 226*, 66−76.

(20) Plotch, S. J., O'Hara, B., Morin, J., Palant, O., LaRocque, J., Bloom, J. D., Lang, S. A. Jr., DiGrandi, M. J., Bradley, M., Nilakantan, R., and Gluzman, Y. (1999) Inhibition of influenza A virus replication by compounds interfering with the fusogenic function of the viral hemagglutinin. *J. Virol. 73*, 140−151.

(21) Staschke, K. A., Hatch, S. D., Tang, J. C., Hornback, W. J., Munroe, J. E., Colacino, J. M., and Muesing, M. A. (1998) Inhibition of influenza virus hemagglutinin-mediated membrane fusion by a compound related to podocarpic acid. *Virology 248*, 264−274.

(22) Hoffman, L. R., Kuntz, I. D., and White, J. M. (1997) Structure-based identification of an inducer of the low-pH conformational change in the influenza virus hemagglutinin: Irreversible inhibition of infectivity. *J. Virol. 71*, 8808−8820.

(23) Matsubara, T., Onishi, A., Saito, T., Shimada, A., Inoue, H., Taki, T., Nagata, K., Okahata, Y., and Sato, T. (2010) Sialic acid-mimic peptides as hemagglutinin inhibitors for anti-influenza therapy. *J. Med. Chem. 53*, 4441−4449.

(24) Feng, F., Miura, N., Isoda, N., Sakoda, Y., Okamatsu, M., Kida, H., and Nishimura, S. (2010) Novel trivalent anti-influenza reagent. *Bioorg. Med. Chem. Lett. 20*, 3772−3776.

(25) Tang, G., Lin, X., Qiu, Z., Li, W., Zhu, L., Wang, L., Li, S., Li, H., Lin, W., Yang, M., Guo, T., Chen, L., Lee, D., Wu, J. Z., and Yang, W. (2011) Design and synthesis of benzenesulfonamide derivatives as potent anti-influenza hemagglutinin inhibitors. *ACS Med. Chem. Lett. 2*, 603−607.

(26) Sawada, T., Fedorov, D. G., and Kitaura, K. (2010) Role of the key mutation in the selective binding of avian and human influenza hemagglutinin to sialosides revealed by quantum-mechanical calculations. *J. Am. Chem. Soc. 132*, 16862−16872.

(27) Takematsu, K., Fukuzawa, K., Omagari, K., Nakajima, S., Nakajima, K, Mochizuki, Y., Nakano, T., Watanabe, H., and Tanaka, S. (2009) Possibility of mutation prediction of influenza hemagglutinin

by combination of hemadsorption experiment and quantum chemical calculation for antibody binding. *J. Phys. Chem. B. 113*, 4991–4994.
(28) Newhouse, E. I., Xu, D., Markwick, P. R., Amaro, R. E., Pao, H. C., Wu, K. J., Alam, M., McCammon, J. A., and Li, W. W. (2009) Mechanism of glycan receptor recognition and specificity switch for avian, swine, and human adapted influenza virus hemagglutinins: a molecular dynamics perspective. *J. Am. Chem. Soc. 131*, 17430–17442.
(29) Kasson, P. M., Ensign, D. L., and Pande, V. S. (2009) Combining molecular dynamics with bayesian analysis to predict and evaluate ligand-binding mutations in influenza hemagglutinin. *J. Am. Chem. Soc. 131*, 11338–11340.
(30) Das, P., Li, J., Royyuru, A. K., and Zhou, R. (2009) Free energy simulations reveal a double mutant avian H5N1 virus hemagglutinin with altered receptor binding specificity. *J. Comput. Chem. 30*, 1654–1663.
(31) Xu, D., Newhouse, E. I., Amaro, R. E., Pao, H. C., Cheng, L. S., Markwick, P. R., McCammon, J. A., Li, W. W., and Arzberger, P. W. (2009) Distinct glycan topology for avian and human sialopentasaccharide receptor analogues upon binding different hemagglutinins: a molecular dynamics perspective. *J. Mol. Biol. 387*, 465–491.
(32) Fleishman, S. J., Whitehead, T. A., Ekiert, D. C., Dreyfus, C., Corn, J. E., Strauch, E. M., Wilson, I. A., and Baker, D. (2011) Computational design of proteins targeting the conserved stem region of influenza hemagglutinin. *Science 332*, 816–821.
(33) Watanabe, K., Sakurai, J., Abe, H., and Katoh, T. (2010) Total synthesis of (+)-stachyflin: a potential anti-influenza A virus agent. *Chem. Commun. 46*, 4055–4057.
(34) Nakatani, M., Nakamura, M., Suzuki, A., Inoue, M., and Katoh, T. (2002) A new strategy toward the total synthesis of stachyflin, a potent anti-influenza A virus agent: concise route to the tetracyclic core structure. *Org. Lett. 4*, 4483–4486.
(35) Carey, J. S., Laffan, D., Thomson, C., and Williams, M. T. (2006) Analysis of the reactions use for the preparation of drug candidate molecules. *Org. Biomol. Chem. 4*, 2337–2347.
(36) Mizukami, T., Imai, J., Hamaguchi, I., Kawamura, M., Momose, H., Naito, S., Maeyama, J., Masumi, A., Kuramitsu, M., Takizawa, K., Nomura, N., Watanabe, S., and Yamaguchi, K. (2008) Application of DNA microarray technology to influenza A/Vietnam/1194/2004 (H5N1) vaccine safety evaluation. *Vaccine 26*, 2270–2283.
(37) Sali, A., and Blundell, T. L. (1993) Comparative protein modelling by satisfaction of spatial restraints. *J. Mol. Biol. 234*, 779–815.
(38) Gamblin, S. J., Haire, L. F., Russell, R. J., Stevens, D. J., Xiao, B., Ha, Y., Vasisht, N., Steinhauer, D. A., Daniels, R. S., Elliot, A., Wiley, D. C., and Skehel, J. J. (2004) The structure and receptor binding properties of the 1918 influenza hemagglutinin. *Science 303*, 1838–1842.
(39) Stevens, J., Corper, A. L., Basler, C. F., Taubenberger, J. K., Palese, P., and Wilson, I. A. (2004) Structure of the uncleaved human H1 hemagglutinin from the extinct 1918 influenza virus. *Science 303*, 1866–1870.
(40) Humphrey, W., Dalke, A., and Schulten, K. (1996) VMD: visual molecular dynamics. *J. Mol. Graph. 14*, 33–38.
(41) The UniProt Consortium. (2011) Ongoing and future developments at the Universal Protein Resource. *Nucleic Acids Res. 39*, D214–D219.
(42) Phillips, J. C., Braun, R., Wang, W., Gumbart, J., Tajkhorshid, E., Villa, E., Chipot, C., Skeel, R. D., Kalé, L., and Schulten, K. (2005) Scalable molecular dynamics with NAMD. *J. Comput. Chem. 26*, 1781–1802.
(43) Feller, S. E., Gawrisch, K., and MacKerell, A. D. (2002) Polyunsaturated fatty acids in lipid bilayers: intrinsic and environmental contributions to their unique physical properties. *J. Am. Chem. Soc. 124*, 318–326.
(44) Jones, G., Willett, P., Glen, R. C., Leach, A. R., and Taylor, R. (1997) Development and validation of a genetic algorithm for flexible docking. *J. Mol. Biol. 267*, 727–748.
(45) Jones, G., Willett, P., and Glen, R. C. (1995) Molecular recognition of receptor sites using a genetic algorithm with a description of desolvation. *J. Mol. Biol. 245*, 43–53.
(46) Verdonk, M. L., Cole, J. C., Hartshorn, M. J., Murray, C. W., and Taylor, R. D. (2003) Improved protein-ligand docking using GOLD. *Proteins: Struct., Funct., Genet. 52*, 609–623.
(47) Mooij, W. T. M., and Verdonk, M. L. (2005) General and targeted statistical potentials for protein-ligand interactions. *Proteins: Struct., Funct., Genet. 61*, 272–281.
(48) Bostrom, J., Greenwood, J. R., and Gottfries, J. (2003) Assessing the performance of OMEGA with respect to retrieving bioactive conformations. *J. Mol. Graphics Modell. 21*, 449–462.
(49) OpenEye Scientific Software, Inc., Santa Fe, NM, USA, www.eyesopen.com.

Regulation of the susceptibility of HIV-1 to a neutralizing antibody KD-247 by nonepitope mutations distant from its epitope

Mari Takizawa[a], Kosuke Miyauchi[a], Emiko Urano[a], Shigeru Kusagawa[a], Katsuhiko Kitamura[b], Satoshi Naganawa[c], Toshio Murakami[d], Mitsuo Honda[e], Naoki Yamamoto[f] and Jun Komano[a]

Objective: A humanized neutralizing antibody, KD-247, targets the V3 loop of HIV-1 Env. HIV-1 bearing the GPGR sequence at the V3 loop is potentially susceptible to KD-247. However, not all GPGR-positive HIV-1 isolates are neutralized by KD-247. We examined the potential mechanism by which the susceptibility of HIV-1 to KD-247-mediated neutralization is regulated.

Design: We searched for nonepitope neutralization regulatory (NNR) mutations that sensitize GPGR-bearing HIV-1_{AD8} to KD-247 and mapped the locations of such mutations relative to the V3 loop.

Methods: We generated a functional HIV-1_{AD8} Env library, and evaluated the viral susceptibility to KD-247 by measuring the half-inhibitory concentration (IC_{50}) to KD-247 on TZM-bl cell assay.

Results: We identified nine KD-247-sensitizing NNR mutations from 30 mutations in various regions of gp120, including the V1/V2 loop, C2, V3 loop, C4, and C5. They specifically affected KD-247-mediated neutralization, as they did not affect the b12-mediated neutralization. When combined, the KD-247-sensitizing NNR mutations additively sensitized the virus to KD-247 by up to 10 000 folds. The KD-247-sensitizing NNR mutations increased KD-247 binding to the virion. Notably, the NNR mutation in C4 coincides with the CD4-binding site of gp120.

Conclusion: Given that most of the KD-247-sensitizing NNR mutations are remote from V3 loop, it is reasonable to hypothesize that the steady-state, local conformation of the V3 loop is regulated by the interdomain contact of gp120. Our mutational analysis complements crystallographic studies by helping provide a better understanding of the steady-state conformation and the functional geometry of Env.

AIDS 2011, **25**:2209–2216

Keywords: envelope, HIV-1, KD-247, neutralization, steady-state conformation

Introduction

HIV-1 is a highly mutagenic virus. The viral envelope glycoprotein gp120/41 (Env) accumulates mutations to escape from the host humoral immunity. The study on HIV-1-neutralizing antibodies (Nabs) and the viral escape from Nab gives us insights into viral pathogenesis, structure–function relationship of Env, and AIDS vaccine design [1–8].

[a]AIDS Research Center, National Institute of Infectious Diseases, Tokyo, [b]Department of Public Health, Yokohama City University School of Medicine, Yokohama, [c]Infectious Disease Regulation Project, The Tokyo Metropolitan Institute of Medical Science, Tokyo, [d]The Chemo-Sero-Therapeutic Research Institute, Kumamoto, [e]Department of Pathology and Microbiology, Division of Microbiology, Nihon University School of Medicine, Tokyo, Japan, and [f]Department of Microbiology, Yong Loo Lin School of Medicine, National University of Singapore, Singapore.

Correspondence to Jun Komano, AIDS Research Center, National Institute of Infectious Diseases, 1-23-1 Toyama Shinjuku, Tokyo 162-8640, Japan.

Tel: +81 3 5285 1111; fax: +81 3 5285 5037; e-mail: ajkomano@nih.go.jp

Received: 8 September 2010; revised: 4 July 2011; accepted: 5 August 2011.

DOI:10.1097/QAD.0b013e32834bab68

A humanized monoclonal Nab, KD-247, which is effective against half of clade B primary HIV-1 isolates, targets the third hypervariable (V3) loop, is an attractive AIDS vaccine target [1–3]. The epitope essential for KD-247-mediated neutralization is the conserved tetrapeptide sequence GPGR (HXB2 coordinate 312–315). A human monoclonal Nab 447–52D targets this same epitope [4]. Mutations in the GPGR sequence confer viral resistance to KD-247 [3,5,6]. Moreover, amino acid changes adjacent to the GPGR motif have also conferred viral resistance to KD-247 (e.g. H, R, and K at 311 position, or P at 316 position) [3]. Such mutations physically interfere with binding to the KD-247 epitope [3]. In the absence of such mutations, HIV-1 bearing the GPGR sequence at the V3 loop is potentially susceptible to KD-247. However, not all GPGR-positive HIV-1 isolates are neutralized by KD-247. The mechanism by which some of the GPGR-bearing viruses are resistant to KD-247 is not fully understood.

We addressed this sequence-neutralization susceptibility discordance by comparing the amino acid sequences of various HIV-1 primary isolates. We defined a virus as resistant to KD-247-mediated neutralization when the half-inhibitory concentration (IC_{50}) was higher than 100 μg/ml. We analyzed V3 loop amino acid sequences from 25 viruses positive for the GPGR epitope, including 11 KD-247-sensitive and 14 KD-247-resistant viruses. Along with the ELISA data in our previous report [3], we found that H304R contributes to KD-247 resistance. The H304R polymorphism accounted for 35.7% (five of 14 isolates) of the examples of sequence-neutralization susceptibility discordance, but all the viruses carrying H304R were CRF01_AE. We failed to identify any neutalization regulatory mutations in the clade B isolates. Additionally, the KD-247 prototype mouse monoclonal antibody C25 was unable to neutralize 17 GPGR-positive HIV-1 clade B primary isolates, even though C25 was able to bind their synthetic V3 loop peptides (unpublished observation). From these data, we postulated that the sequence-neutralization susceptibility discordance is due to non-epitope neutralization regulatory (NNR) mutations, especially remote from the V3 loop. Such NNR mutations would be positioned at certain key sites within the Env domains and regulate the steady-state conformation. NNR mutations have been predicted for 447–52D and other cross-reactive Nab [6–11]. To test this hypothesis, we examined 15 entire Env amino acid sequences of KD-247-sensitive and KD-247-resistant viruses. However, we were unable to identify amino acids associated with susceptibility to KD-247. This suggests that the heterologous virus approach is not sensitive enough to identify NNR mutations because the diversity of Env amino acid sequences is beyond the level of detection.

Here we employed a genetic approach to identify NNR mutations using the HIV-$1_{AD8/ADA}$ (AD8 hereafter), which displays the sequence-neutralization susceptibility discordance. The AD8 strain has been reported to be sensitive to 447–52D, which targets the same neutralization epitope as KD-247 within the V3 loop [10], suggesting that the GPGR epitope of the V3 loop is open to antibodies. We thought that this should help understand how the NNR mutations work. It does not contain insertions adjacent to the GPGR motif, as HIV-1_{HXB2} or HIV-1_{NL4-3} do (QR insertion before I and G) nor H304R. Only a few NNR mutations that make HIV-1 resistant to KD-247 have been reported in the V1/V2 loop [6]. In this work, we generated a functional AD8 Env library to identify many NNR mutations simultaneously that cause HIV-1 to become susceptible to KD-247. Through KD-247-sensitizing NNR mutations, we tried to understand the regulatory mechanism of the viral susceptibility to KD-247-mediated neutralization.

Materials and methods

Cells, viruses, and transfection

Cells were maintained in RPMI-1640 Medium (Sigma, St Louis, Missouri, USA) supplemented with 10% fetal bovine serum (FBS) (Japan Bioserum, Tokyo, Japan), 50 U/ml penicillin, and 50 μg/ml streptomycin (Invitrogen, Tokyo, Japan), at 37°C in a humidified 5% CO_2 atmosphere. Cells were transfected with Lipofectamine 2000 according to the manufacturer's protocol (Invitrogen). The other viruses and TZM-bl cells were obtained from the NIH AIDS Research and Reference Reagent Program.

Antibodies

KD-247 was provided by the Chemo-Sero-Therapeutic Research Institute, and b12 is a generous gift from Dr Burton (The Scripps Research Institute).

Cloning

AD8 Env was amplified by nested reverse-transcriptase-PCR using RNA extracted from the culture supernatant as a template (RNeasy mini kit; Qiagen, Hilden, Germany). The primers used were as follows. For the first PCR, the sense primer was 5′-ATG AAA CTT ACG GGG ATA CTT GGG-3′ (HXB2 nucleotide coordinates 5698–5721) and the antisense primer was 5′-GGT ACT AGC TTG AAG CAC CAT CC-3′ (HXB2 nucleotide coordinates 9236–9214); and for the nested PCR, the sense primer was 5′-ATA AGA ATT CTG CAA CAA CTG CTG-3′ (HXB2 nucleotide coordinates 5739–5762) and the antisense primer was 5′-TTC CAG GTC TCG AGA TGC TGC-3′ (HXB2 nucleotide coordinates 8910–8890). EcoRI-XhoI fragments of the PCR products were cloned into the corresponding restriction sites of pNL4–3. The *env* gene was sequenced using the following primers: 3479a, 5′-CTT GGG ATG TTG

ATG ATC TGT AGT GCT GTA GA-3′; 003A, 5′-AGC AGA AGA CAG TGG CAA TG-3′; 106A, 5′-CAT ACA TTA TTG TGC CCC GGC TGG-3′; 545A, 5′-GAC AAT TGG AGA AGT GAA TT-3′; and 5700, 5′-AGC CTG TGC CTC TTC AGC TAC CAC CGC TTG-3′.

Neutralization assay

To produce virus from proviral DNA, 293FT cells (Cat# R700–007; Invitrogen) grown in six-well plates were transfected with proviral DNA-encoding plasmid (1 μg) using Lipofectamine 2000, and replated into a six-well plate at 4–6 h posttransfection. At 48 h posttransfection, the cell culture medium was collected and mixed with dextran (final concentration 16.25 μg/ml, DEAE-Dextran chloride, molecular weight ~500 kDa; ICN Biomedicals Inc., Aurora, Ohio, USA). The TZM-bl cells were plated in 96-well plates at 500 cells per well in a volume of 100 μl a day before infection. The virus and KD-247 were mixed in a volume of 50 μl and incubated at 37°C for 30 min. Then, the TZM-bl cells were exposed to the virus-KD-247 mixture. At 3 days postinfection, luciferase activity was measured using the Steady-Glo Luciferase Assay system (Promega, Madison, Wisconsin, USA). The IC_{50} was defined as the Nab concentration that yielded a half-reduction in luciferase activity compared with the control wells after subtracting background signals as previously described [12]. Luminescence was detected using a Veritas Microplate Luminometer (Promega). The GHOST cell-based and peripheral blood mononuclear cell-based neutralization assays were performed as described previously [3].

Virus capture ELISA

The ELISA plate (Nunclon, Roskilde, Denmark) was coated by KD-247 with incubating plates with 100 μl of KD-247 preparation (10 μg/ml) in a carbonate buffer (15 mmol/l Na_2CO_3, 35 mmol/l $NaHCO_3$, pH 9.6) at 4°C overnight. Plates were washed five times with Plate Wash Buffer (Zeptometrics, Buffalo, New York, USA), and blocked with PBS containing 20% FBS (Nalgene, Rochester, New York) at 37°C for 1 h. After washing the plates for five times with Plate Wash Buffer and once with PBS, virus was captured by KD-247 by incubating plates with viral preparations containing 50 ng of $p24^{CA}$ resuspended in a volume of 100 μl PBS. After washing PBS with 10% FBS, captured virus was lysed in a buffer and a $p24^{CA}$ ELISA was conducted according to the manufacturer's protocol (Zeptometrics).

Results

Construction of a functional Env library based on the AD8 strain

In theory, it is possible to identify NNR mutations conferring viral resistance to the Nab by selecting Nab-resistant mutants from a Nab-sensitive virus in culture. However, this approach is not ideal for the identification of many NNR mutations at the same time because it primarily selects epitope mutants and only a few dominant NNR mutants. To overcome this problem, we tried to identify NNR mutations that sensitize HIV-1 to KD-247. To achieve this goal, we generated a functional Env library and tried to identify KD-247-sensitizing NNR mutations by correlating mutations with viral susceptibility to KD-247-mediated neutralization. We chose a KD-247-resistant strain, AD8, that shows sequence-neutralization susceptibility discordance, and its IC_{50} to KD-247, when the virus is produced in 293T cells from a proviral DNA, was 354.9 μg/ml by TZM-bl assay (average of five independent experiments). Interestingly, this strain has been reported to be sensitive to 447–52D, which targets the same neutralization epitope within the V3 loop [10]. This suggests that the GPGR epitope of the V3 loop is open to antibodies, and the hindrance of KD-247 epitope is unlikely.

An Env mutant library can be produced by genetic engineering (e.g., PCR-based random mutagenesis). However, such an approach does not always produce functional Env. In contrast, Env mutants generated by viral diversification in tissue culture should be functional unless sporadic mutations that interfere with Env function are introduced. We took the latter approach to generate a functional Env library. We diversified AD8 viruses by approximately 100 passages in MOLT-4 cells. This was a simple bulk passage of virus, whereby tissue culture supernatant was transferred to fresh cells, likely conferring the survival of random mutations. We examined the diversity by sequencing 56 *env* clones. Of these 56 clones, 54 *env* clones were independent, suggesting that the diversification of *env* was successful. The IC_{50} of diversified AD8 to KD-247 was 334.6 μg/ml by TZM-bl assay (average of three independent experiments), suggesting that the diversified AD8 is resistant to KD-247 when scored in bulk. Our data indicate that long-term viral selection in tissue culture does not necessarily select a few dominant mutants; various mutants of independent origins can be maintained. We expected that most of the amino acid substitution mutations should not damage Env function; otherwise, they should not have been selected in culture. The average number of mutations was 3.0 per clone, including the frameshift and stop codon mutations, and, importantly, every virus retained the GPGR epitope in the V3 loop. These viruses were distinct from each other but not as divergent as a panel of field isolates, making them suitable for the identification of KD-247-sensitizing NNR mutations. Our diversification protocol does not necessarily select Env mutants with higher or lower susceptibility to KD-247. We expect that some (but not all) mutations may increase the susceptibility to KD-247. We next evaluated whether any mutations could confer the increased susceptibility of the AD8 strain to KD-247.

Identification of nonepitope neutralization regulatory mutations in various domains of gp120

In our viral diversification protocol, mutations can occur in any region of the viral genome. We are concerned that non-Env mutations could affect neutralization susceptibility to KD-247. For example, the IC_{50} could be scored lower if the viral fitness is poor and higher if viral fitness is high. To avoid these possibilities, we cloned diversified Env into the same viral genetic background. We chose HIV-1_{NL4-3} because it is one of the standard molecular clones of HIV-1, and the proviral DNA is relatively stable and, thus, suitable for such cloning. The AD8 *env* cloned HIV-1_{NL4-3} was named NL/AD8. At first, we verified that the susceptibility of viral isolates to KD-247-mediated neutralization could be reproduced on the HIV-1_{NL4-3} genetic background. For this purpose, we used HIV-1_{MN} and AD8 Env, which are highly susceptible and resistant to KD-247, respectively. Cloning *env* from KD-247-sensitive HIV-1_{MN} into HIV-1_{NL4-3} reproduced neutralization susceptibility (IC_{50} 0.07 μg/ml). Similarly, the KD-247 resistance seen in the AD8 strain was reproduced in the NL/AD8 viruses (IC_{50} 357.5 μg/ml, Table 1). Env mutants with no stop codon or frameshift were tested on the HIV-1_{NL4-3} background. Chimeric viruses carrying AD8 Env mutants that did not yield and infectivity index in TZM-bl cells comparable to that of viruses carrying NL4–3/AD8 were not tested further. Viruses bearing combinations of mutations were generated by positioning mutations between useful restriction enzyme recognition sites in the viral genome. Finally, we examined 27 molecular clones by substituting HIV-1_{NL4-3} *env* with the diversified AD8 *env* clones or AD8 *env* with a point mutation found in the diversified pool (Table 1) Mutations causing Env amino acid changes did not comutate the viral proteins encoded in the Env-overlapping frames including *vpu*, *tat*, and *rev*.

We determined the IC_{50} of KD-247 on these viruses using TZM-bl cells. Out of 27 viruses, 19 increased their susceptibility to KD-247-mediated neutralization to more than two-fold that of NL/AD8 (19 of 27 clones, 70.4%; Table 1), consistent with previous reports suggesting that the long-term passages *in vitro* select Nab-susceptible HIV-1 [13,14]. Comparing the IC_{50} for each of the mutations, we identified nine NNR mutations that sensitized viruses to KD-247 by more than two-fold (nine of 30 mutations, 30.0%; Table 2). A mutation that altered the IC_{50} no more than two-fold was defined as a non-NNR mutation. Seventeen

Table 1. Summary of half-inhibitory concentration of mutant viruses against KD-247 and b12.

Mutations[a]	KD-247		b-12	
	IC_{50} (μg/m)[b]	Fold sensitization[c]	IC_{50} (μg/m)[b]	Fold sensitization[c]
NL/AD8	357.5 ± 121.8	1	2.4 ± 1.0	1
T48A, D163N, R248M, N297S, S370N, A721T	0.03 ± 0.02	12 342.2	0.2 ± 0.1	12.6
T48A, S186R, S302G S370N, F764S*	7.0 ± 5.5	50.8	0.7 ± 0.2	3.3
S370N, K428E, Q504R, A509T, G689S	39.8 ± 25.9	9.0	1.0 ± 0.3	2.3
D163G, R300G, S370N, S760G	4.4 ± 3.9	82.1	0.4 ± 0.1	6.0
K285R, N298Y, I488T, E506K	480.9 ± 27.1	0.7	1.8 ± 1.1	1.3
E31G, T48A, N279T	141.4 ± 53.1	2.5	1.0 ± 0.2	2.5
D181G, N298Y, S760G	350.0 ± 173.2	1.0	1.8 ± 0.9	1.3
S186R, S370N, S760G	102.8 ± 8.1	3.5	NT	
N298Y, S370N, S760G	380.9 ± 70.7	0.9	1.9 ± 1.0	1.3
V178A, N298Y	89.0 ± 29.3	4.0	8.7 ± 0.9	0.3
N191D, N298Y	157.2 ± 76.8	2.3	1.5 ± 0.9	1.6
I280M, S370N	284.6 ± 34.3	1.3	6.4 ± 0.5	0.4
N297S, S370N	2.4 ± 1.8	149.0	0.8 ± 0.2	3.0
N298Y, E655G*	428.1 ± 47.5	0.8	1.1 ± 0.0	2.3
S370N, N391S	280.5 ± 29.6	1.3	2.5 ± 1.9	1.0
S370N, I546V	303.6 ± 60.8	1.2	2.0 ± 0.2	1.2
S370N, A580T	81.3 ± 18.0	4.4	2.6 ± 0.7	0.9
D163G	6.0 ± 3.5	59.4	1.3 ± 0.0	1.9
D163N	4.8 ± 2.4	74.3	0.9 ± 0.4	2.6
S186R	46.7 ± 24.4	7.7	1.0 ± 0.3	2.4
R248M	59.7 ± 35.8	6.0	2.6 ± 0.7	0.9
N297S	3.0 ± 1.4	119.2	1.2 ± 0.5	2.1
R300G	68.8 ± 28.1	5.2	2.2 ± 1.2	1.1
S302G	6.6 ± 3.4	54.4	2.2 ± 1.1	1.1
S370N	211.5 ± 92.1	1.7	1.2 ± 0.5	2.0
K428E	39.3 ± 35.0	9.1	2.1 ± 0.1	1.2
Q504R	121.6 ± 38.5	2.9	2.7 ± 1.0	0.9

IC_{50}, half-inhibitory concentration; NT, not tested.
[a]NL/AD8 was used as a reference. The amino acid numbering is according to HIV-1AD8 Env. The virus without an asterisk was subjected to virus–antibody binding experiment shown in Fig. 1.
[b]The average and SD from two to 13 independent experiments are shown.
[c]The IC_{50} of the control virus was divided by IC_{50} of each mutant.

Table 2. Summary of mutations characterized in this study.

Mutations[b]	HXB2 coordinate	Location in Env[a]	Fold sensitization
NNR			
D163G	G167	V1/V2	59.4
D163N	G167	V1/V2	74.3
S186R	K192	V1/V2	7.7
R248N	R252	C2	7.0
N297S	N301	V3	119.2
R300G	R304	V3	5.2
S302G	R306	V3	54.4
K428E	K432	C4	9.1
Q504R	Q507	C5	2.9
Non-NNR			
E31G[c]	E32	C1	–
T48A[c]	T49	C1	–
V178A[c]	I181	V1/V2	–
D181G	D185	V1/V2	–
N191D[c]	S195	V1/V2	–
K285R	N289	V3	–
N298Y	N302	V3	–
S370N	S375	C3	–
N391S	X396	V4	–
I488T	I491	C5	–
E506K	E509	C5	–
A509T[c]	A512	gp41	–
I546V	I548	gp41	–
A580T[c]	A582	gp41	–
E655G	E657	gp41	–
G689S[c]	G691	gp41	–
S760G	S762	gp41	–

NNR, nonepitope neutralization regulatory.
[a]The gp120 was subdivided into C1, V1/V2, C3, V3, C4, V4, and C5.
[b]NNR mutations conferring a change in neutralization susceptibility of more than two-fold. Non-NNR mutations are defined as mutations conferring a change in neutralization susceptibility of no more than two-fold.
[c]Estimated from the fold sensitization of a mutant carrying multiple mutations.

non-NNR mutations were also found (Table 2). The magnitude of sensitization by NNR mutations ranged from 2.9 to 119.2. These NNR mutations were present in a broad range of gp120 sites, including V1/V2 loop, C2, V3 loop, C4, and C5. When combined, the NNR mutations additively sensitized the virus to KD-247 by up to 10 000-fold, suggesting an independent structural cross-talk between the V3 loop and each NNR mutation. Such a drastic effect was not observed against b12 Nab targeting the CD4-binding site of gp120 (Table 1). The effect of these NNR mutations appeared to be specific to KD-247, as evidenced by the statistically insignificant correlation between IC_{50} values for KD-247 and b12 (Supplementary Information S1, http://links.lww.com/QAD/A180). This is probably due to the conserved nature of the b12 epitope structure and function. It should be noted that infection with mutant viruses yielded similar levels of luciferase signal from TZM-bl cells when comparable amounts of viruses were used. Also, the viruses bearing six mutations (T48A, D163N, R248M, N297S, S370N, and A721T) replicated in MOLT-4/CCR5 cells with similar efficiency to the no mutation control (NL/AD8), suggesting that replication competency can not account for the change in neutralization susceptibility (data not shown).

Correlation between neutralization susceptibility and KD-247 binding affinity to the virion

We investigated how NNR mutations could sensitize a virus to KD-247-mediated neutralization. We tested whether the KD-247-sensitizing NNR mutation could induce a conformational change in gp120 in such a way that KD-247 became able to bind to gp120 with higher efficiency. To address this question, we performed a capture ELISA in which ELISA plates were precoated with KD-247 and blocked, followed by incubation of virions bearing NNR mutations in the wells of the ELISA plate. The amount of KD-247 captured virus was quantified by ELISA detecting the viral core antigen (Fig. 1). If the latter model is correct, KD-247 captures every mutant with similar efficiencies. As a result, viral binding to KD-247 was significantly correlated with neutralization susceptibility ($P < 0.01$, $n = 26$, two-tailed Student's *t*-test; Fig. 1). These data support a model in which KD-247-sensitizing NNR mutations alter the steady-state structure of gp120 into a conformation such that KD-247 is able to bind to its target with higher efficiencies.

Structural analysis of nonepitope neutralization regulatory mutations

To gain insight into the potential mechanisms whereby KD-247-sensitizing mutations enable neutralization of virions, we used the three-dimensional structural model described by Blay *et al.* [15]. We used an X-ray crystallographic structure with variable loops [15], which was aligned in a trimeric form in accordance with a model developed by Pancera *et al.* [16].

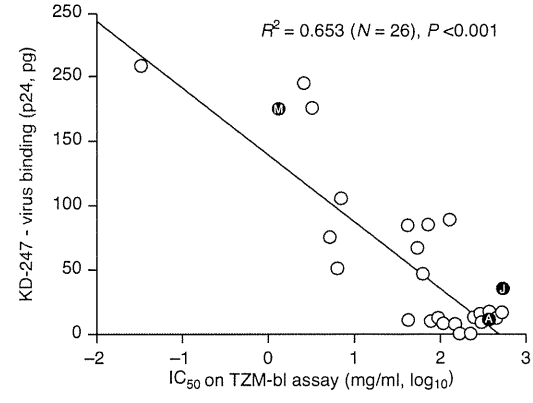

Fig. 1. Analysis of neutralization susceptibility of HIV-1 to KD-247. The half-inhibitory concentration (IC_{50}) for each virus for KD-247 is plotted against the virus capture ELISA data using KD-247 as summarized in Table 1. A significant correlation between the two parameters was detected ($P < 0.01$, two-tailed Student's *t*-test). HIV-1_{MN}, HIV-1_{JR-FL}, and HIV-$1_{NL/AD8}$ are shown as M, J, and A, respectively.

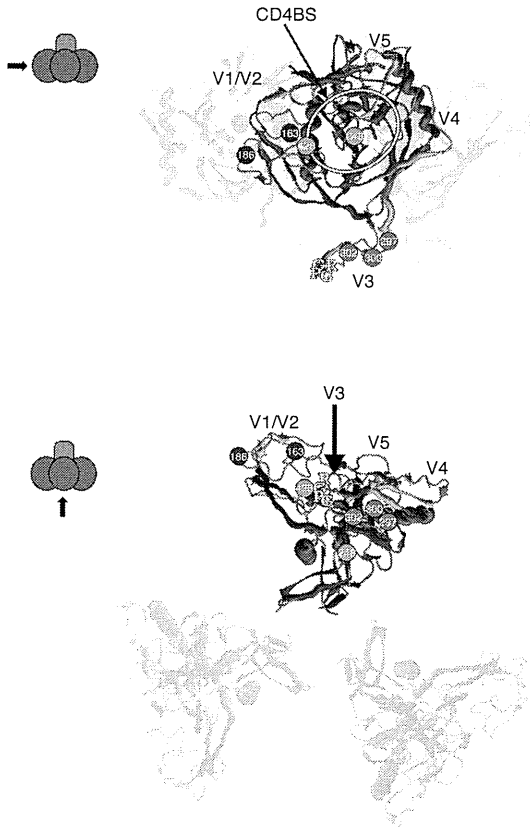

Fig. 2. The three-dimensional mapping of KD-247-sensitizing non-epitope neutralization regulatory mutations based on the Env structure aligned in a trimeric form. The view angle is indicated on the left (arrows) where the gp120 and gp41 are shown in sphere (purple) and rectangle (red), respectively. The gp120 core was shown in blue and red, and the variable loops are shown in yellow. KD-247-sensitizing non-epitope neutralization regulatory (NNR) mutations are indicated by their amino acid numbers. The NNR mutations on the V1/V2 loop, V3 loop, and gp120 core are shown in blue, red, and green, respectively. The GPGR on the V3 loop is shown as a letter code in yellow. The approximate CD4-binding site (CD4BS) is indicated by a white line. The original structural image was developed by Blay *et al.* [15]

The R248N in the C2 region is placed on the gp41 side of the gp120 surface and is not facing the trimeric interface of gp120 (Fig. 2, green) [15]. It has been reported that the H66N, positioned near the trimeric interface of gp120, induces a conformational change of gp120 [17,18]. It has been proposed that H66N alters the quaternary Env structure by acting intermolecularly rather than intramolecularly. In contrast to H66N, the R248N is not positioned at or close to the trimeric surface of gp120. It is likely that R248N induces a different conformational change of the gp120 from H66N, one that does not affect the neutralization susceptibility to b12. It is of interest that the remote KD-247-sensitizing NNR mutation of the gp120 core can specifically affect the conformation of the V3 loop positioned on the gp120 surface.

K428E in the C4 region was mapped in the CD4-binding site close to the so-called bridging sheet (Fig. 2, green), suggesting that the V3 loop and CD4-binding site neutralization epitopes can influence each other's conformation under steady-state conditions. Like R248N, K428E is not positioned at or close to the gp120 trimeric interface. Thus, we speculate that K428E induces a local, not global, Env conformational change. The amino acid corresponding to K428 has been implicated previously in b12 binding through its side-chain as well as through CD4, using HXBc2 Env as a model [19,20]. K428E induces a drastic change in side-chain properties. However, K428E did not significantly affect the viral susceptibility to b12 and the replication efficiency of the NL/AD8 backbone, suggesting that this amino acid may not play a significant role in AD8 Env–b12 interaction. K428 is positioned at the edge of the b12–Env or CD4–Env contact region and, thus, may not contribute significantly to b12–Env or CD4–Env interaction in the context of AD8 Env. Structural cross-talk between the V3 loop and the C4 region under steady-state conditions has been suggested by two studies using monoclonal antibodies. Our approach pinpointed the amino acids responsible for this inter-domain cross-talk.

In contrast to the above two mutations, the precise positioning of KD-247-sensitizing NNR mutations in the V1/V2 and V3 loop is unclear because structural information for them are lacking in the original crystallographic data. According to the molecular dynamics modeling [15], the KD-247-sensitizing NNR mutations in the V1/V2 and V3 loop may not be positioned at or close to the trimeric surface of gp120 (Fig. 2). Instead, they function intramolecularly to affect the conformation of the KD-247 epitope. The Q504R is also lacking in the X-ray crystal structures. However, Q504R is next to the gp120/41 cleavage site and should be close to gp41. The gp41 is relatively proximal to the CD4-binding site of gp120. Some of the mutations in gp41, including T569A and I675V, have been reported to influence the viral susceptibility to Nabs, including b12 [21]. It is conceivable that these mutations in gp41 affect the conformation of gp120. In contrast to T569A and I675V, Q504R is not a b12-sensitizing NNR mutation. Therefore, the conformational change of gp120 induced by Q504R should be distinct from the gp41 mutations.

The structural approach has a potential limitation because the molecular model of Env does not represent the native structure but the liganded structure (Fig. 2). In fact, almost all of the deposited X-ray crystallographic structures are devoid of V1/V2 and/or V3 loops and do not represent the native Env structure, including

the model that our figure is built upon [4,8,15,16,19,22–24].

Discussion

In this work, we identified a number of KD-247-sensitizing NNR mutations using a functional Env library. We re-examined KD-247-sensitive or KD-247-resistant GPGR-positive HIV-1 isolates for NNR mutations and found that KD-247-sensitive viruses, MN (a tissue culture adapted strain of MN) and MNp (a primary HIV-1 isolate), had the mutation equivalent to N301S [25,26]. The predictive value for KD-247 susceptibility due to this mutation was high in the clade B population. However, this does not apply to CRF01_AE, suggesting that this mutation is a clade B-specific predictor of viral susceptibility to KD-247. The other KD-247-sensitizing NNR mutations identified in AD8 did not fully account for the neutralization susceptibility of all of the HIV-1 primary isolates. This suggested that additional NNR mutations should be present, and/or NNR mutations in a given individual virus may function differently than in the other viruses.

How do these mutations alter the conformation of Env to increase the susceptibility of virus to KD-247-mediated neutralization? AD8 is originally resistant to KD-247. One of the molecular mechanisms of AD8 resistance to KD-247 is an epitope-masking by other gp120 domains, possibly the V1/V2 loop or polysaccharides attached to the gp120 [6,27]. Recently, however, Gorny *et al.* [28] reported that the V3 loop of AD8 Env is accessible to KD-247, as AD8 is susceptible to 447–52D-mediated neutralization. This clearly suggests that the sensitization of AD8 strain to KD-247 by the NNR mutations we identified is unlikely due to the removal of the Env domains that physically block antibody access to GPGR epitope. We assume that the V3 loop forms a local conformation in which the neutralization epitope of KD-247 is buried or cannot be recognized by a Nab (local epitope conformation model). When the KD-247-sensitizing NNR mutation occurs, it induces a local, not a global, conformational change of the V3 loop that exposes the neutralization epitope of KD-247. Most of the KD-247-sensitizing NNR mutations are remote from V3 loop. Thus, we assume that KD-247-sensitizing NNR mutations may be located at or close to the interdomain contact regions, and regulate the local conformation of the V3 loop indirectly. Although proven by X-ray crystallographic studies, we propose that the steady-state Env structure is regulated such a way that the domain-independent structural fluctuation is limited. This model predicts that the steady-state structure of the V3 loop is relatively rigid and that its local conformational fluctuation is restricted. This model is relevant to understand the mechanism of action of other NNR mutations against array of Nabs [6–11].

Much attention has been paid to the structural dynamics of HIV-1 Env on CD4 and/or Nab binding. In contrast, not as much attention has been paid to the steady-state conformational dynamics of Env. Unlike previous studies, ours focuses on the steady-state conformational regulation of Env. X-ray crystallography is the best approach to solve a high-resolution native Env structure. However, technical hurdles prevent us from doing so for HIV-1 Env. We examined the mechanism by which the Env conformation is regulated by utilizing Nab KD-247 as a probe. Our approach to identify NNR mutations should complement the crystallization approach in achieving a better understanding of the steady-state structure of HIV-1 Env. Revealing the native structure of Env is critical to the design of an immunogen for the AIDS vaccine and to an understanding of how Env supports virus–cell membrane fusion from the receptor-unbound state.

Acknowledgements

The authors would like to thank Dr Nancy Haigwood for kindly providing the Env structural data. M.T., K.M., E.U., S.K., K.K., S.N., and J.K. designed and performed experiments. T.M., M.H., N.Y., and J.K. analyzed data. J.K. wrote the manuscript.

Conflicts of interest

This work was supported in part by the Japan Health Science Foundation, the Japanese Ministry of Health, Labor and Welfare (H18-AIDS-W-003 and H20-AIDS-G-008 to JK), and the Japanese Ministry of Education, Culture, Sports, Science and Technology (18689014 and 18659136 to J.K.).

There are no conflicts of interest.

References

1. Euler Z, Bunnik EM, Burger JA, Boeser-Nunnink BD, Grijsen ML, Prins JM, *et al.* **Activity of broadly neutralizing antibodies, including PG9, PG16 and VRC01, against recently transmitted subtype B HIV-1 variants from early and late in the epidemic.** *J Virol* 2011; **85**:7236–7245.
2. Hartley O, Klasse PJ, Sattentau QJ, Moore JP. **V3: HIV's switch-hitter.** *AIDS Res Hum Retroviruses* 2005; **21**:171–189.
3. Moore PL, Gray ES, Morris L. **Specificity of the autologous neutralizing antibody response.** *Curr Opin HIV AIDS* 2009; **4**:358–363.
4. Moscoso CG, Sun Y, Poon S, Xing L, Kan E, Martin L, *et al.* **Quaternary structures of HIV Env immunogen exhibit conformational vicissitudes and interface diminution elicited by ligand binding.** *Proc Natl Acad Sci U S A* 2011; **108**:6091–6096.
5. Walker LM, Phogat SK, Chan-Hui PY, Wagner D, Phung P, Goss JL, *et al.* **Broad and potent neutralizing antibodies from an African donor reveal a new HIV-1 vaccine target.** *Science* 2009; **326**:285–289.

6. Walker LM, Burton DR. **Rational antibody-based HIV-1 vaccine design: current approaches and future directions.** *Curr Opin Immunol* 2010; **22**:358–366.
7. Willey S, Aasa-Chapman MM. **Humoral immunity to HIV-1: neutralization and antibody effector functions.** *Trends Microbiol* 2008; **16**:596–604.
8. Zhou T, Georgiev I, Wu X, Yang ZY, Dai K, Finzi A, *et al.* **Structural basis for broad and potent neutralization of HIV-1 by antibody VRC01.** *Science* 2010; **329**:811–817.
9. Wei X, Decker JM, Wang S, Hui H, Kappes JC, Wu X, *et al.* **Antibody neutralization and escape by HIV-1.** *Nature* 2003; **422**:307–312.
10. Gorny MK, Revesz K, Williams C, Volsky B, Louder MK, Anyangwe CA, *et al.* **The v3 loop is accessible on the surface of most human immunodeficiency virus type 1 primary isolates and serves as a neutralization epitope.** *J Virol* 2004; **78**:2394–2404.
11. Gray ES, Moore PL, Bibollet-Ruche F, Li H, Decker JM, Meyers T, *et al.* **4E10-resistant variants in a human immunodeficiency virus type 1 subtype C-infected individual with an antimembrane-proximal external region-neutralizing antibody response.** *J Virol* 2008; **82**:2367–2375.
12. Martin L, Stricher F, Misse D, Sironi F, Pugnière M, Barthe P, *et al.* **Rational design of a CD4 mimic that inhibits HIV-1 entry and exposes cryptic neutralization epitopes.** *Nat Biotechnol* 2003; **21**:71–76.
13. Wrin T, Loh TP, Vennari JC, Schuitemaker H, Nunberg JH. **Adaptation to persistent growth in the H9 cell line renders a primary isolate of human immunodeficiency virus type 1 sensitive to neutralization by vaccine sera.** *J Virol* 1995; **69**:39–48.
14. Zhang YJ, Fredriksson R, McKeating JA, Fenyo EM. **Passage of HIV-1 molecular clones into different cell lines confers differential sensitivity to neutralization.** *Virology* 1997; **238**:254–264.
15. Blay WM, Gnanakaran S, Foley B, Doria-Rose NA, Korber BT, Haigwood NL. **Consistent patterns of change during the divergence of human immunodeficiency virus type 1 envelope from that of the inoculated virus in simian/human immunodeficiency virus-infected macaques.** *J Virol* 2006; **80**:999–1014.
16. Pancera M, Majeed S, Ban YE, Chen L, Huang CC, Kong L, *et al.* **Structure of HIV-1 gp120 with gp41-interactive region reveals layered envelope architecture and basis of conformational mobility.** *Proc Natl Acad Sci U S A* 2010; **107**:1166–1171; Epub 2010 Dec 28..
17. Kassa A, Finzi A, Pancera M, Courter JR, Smith AB 3rd, Sodroski J. **Identification of a human immunodeficiency virus type 1 envelope glycoprotein variant resistant to cold inactivation.** *J Virol* 2009; **83**:4476–4488.
18. Kassa A, Madani N, Schon A, Haim H, Finzi A, Xiang SH, *et al.* **Transitions to and from the CD4-bound conformation are modulated by a single-residue change in the human immunodeficiency virus type 1 gp120 inner domain.** *J Virol* 2009; **83**:8364–8378.
19. Zhou T, Xu L, Dey B, Hessell AJ, Van Ryk D, Xiang SH, *et al.* **Structural definition of a conserved neutralization epitope on HIV-1 gp120.** *Nature* 2007; **445**:732–737.
20. Wu X, Zhou T, O'Dell S, Wyatt RT, Kwong PD, Mascola JR. **Mechanism of human immunodeficiency virus type 1 resistance to monoclonal antibody B12 that effectively targets the site of CD4 attachment.** *J Virol* 2009; **83**:10892–10907.
21. Blish CA, Nguyen MA, Overbaugh J. **Enhancing exposure of HIV-1 neutralization epitopes through mutations in gp41.** *PLoS Med* 2008; **5**:e9.
22. Cho YK, Foley BT, Sung H, Kim YB, Kim JH. **Molecular epidemiologic study of a human immunodeficiency virus 1 outbreak in haemophiliacs B infected through clotting factor 9 after 1990.** *Vox Sang* 2007; **92**:113–120.
23. Huang CC, Tang M, Zhang MY, Majeed S, Montabana E, Stanfield RL, *et al.* **Structure of a V3-containing HIV-1 gp120 core.** *Science* 2005; **310**:1025–1028.
24. Diskin R, Marcovecchio PM, Bjorkman PJ. **Structure of a clade C HIV-1 gp120 bound to CD4 and CD4-induced antibody reveals anti-CD4 polyreactivity.** *Nat Struct Mol Biol* 2010; **17**:608–613.
25. Leavitt M, Park EJ, Sidorov IA, Dimitrov DS, Quinnan GV Jr. **Concordant modulation of neutralization resistance and high infectivity of the primary human immunodeficiency virus type 1 MN strain and definition of a potential gp41 binding site in gp120.** *J Virol* 2003; **77**:560–570.
26. Eda Y, Takizawa M, Murakami T, Maeda H, Kimachi K, Yonemura H, *et al.* **Sequential immunization with V3 peptides from primary human immunodeficiency virus type 1 produces cross-neutralizing antibodies against primary isolates with a matching narrow-neutralization sequence motif.** *J Virol* 2006; **80**:5552–5562.
27. Kwong PD, Wyatt R, Robinson J, Sweet RW, Sodroski J, Hendrickson WA. **Structure of an HIV gp120 envelope glycoprotein in complex with the CD4 receptor and a neutralizing human antibody.** *Nature* 1998; **393**:648–659.
28. Gorny MK, Williams C, Volsky B, Revesz K, Cohen S, Polonis VR, *et al.* **Human monoclonal antibodies specific for conformation-sensitive epitopes of V3 neutralize human immunodeficiency virus type 1 primary isolates from various clades.** *J Virol* 2002; **76**:9035–9045.

DOI: 10.1002/cmdc.201100542

A Synthetic C34 Trimer of HIV-1 gp41 Shows Significant Increase in Inhibition Potency

Wataru Nomura,[a] Chie Hashimoto,[a] Aki Ohya,[a] Kosuke Miyauchi,[b] Emiko Urano,[b] Tomohiro Tanaka,[a] Tetsuo Narumi,[a] Toru Nakahara,[a] Jun A. Komano,[b] Naoki Yamamoto,[c] and Hirokazu Tamamura*[a]

The development of new anti-HIV-1 drugs such as inhibitors of protease and integrase has been contributed to highly active anti-retroviral therapy (HAART) for the treatment of AIDS.[1] The entry of human immunodeficiency virus type 1 (HIV-1) into target cells is mediated by its envelope glycoprotein (Env), a type I transmembrane protein that consists of surface subunit gp120 and noncovalently associated transmembrane subunit gp41.[2] Sequential binding of HIV-1 gp120 to its cell receptor CD4 and a co-receptor (CCR5 or CXCR4) can trigger a series of conformational rearrangements in gp41 to mediate fusion between viral and cellular membranes.[3–5] The protein gp41 is hidden beneath gp120, and its ectodomain contains helical N- and C-terminal leucine/isoleucine heptad repeat domains, N-HR and C-HR. Particular regions of N-HR and C-HR are involved in membrane fusion, and 36-mer and 34-mer peptides, which are derived from N-HR and C-HR, have been designated as the N-terminal helix (N36) and C-terminal helix (C34), respectively. In the membrane fusion of HIV-1, these helices assemble to form a six-helical bundle (6-HB) consisting of a central parallel trimer of N36 surrounded by C34 in an antiparallel hairpin fashion. Synthetic peptides derived from these helices have potent antiviral activity against both laboratory-adapted strains and primary isolates of HIV-1.[6–9] They inhibit the membrane fusion stage of HIV-1 infection in a dominant-negative manner by binding to the counterpart regions of gp41 (N-HR or C-HR), blocking formation of the viral gp41 core.

Several potent anti-HIV-1 peptides based on the C-HR region have been discovered,[7,8] and T20 was subsequently developed as the clinical anti-HIV-1 drug enfuvirtide (Roche/Trimeris).[8,10–13] It is a 36-mer peptide derived from the gp41 C-HR sequence and can bind to the N-HR to prevent formation of the 6-HB in a dominant-negative fashion.[10] T20 therapy has brought safety, potent antiretroviral activity, and immunological benefit to patients, but its clinical application is limited by the development of resistance. The C-terminal helix C34 is also a C-HR-derived peptide, and contains the amino acid residues required for docking into the hydrophobic pocket, termed the "deep pocket", of the trimer of the N-HR region. This peptide potently inhibits HIV-1 fusion in vitro.[14] To date, several gp41 mimetics, especially those of N36 regions, which assemble these helical peptides with branched peptide linkers, have been synthesized as antigens.[15–19]

Recently, by using a novel template with C3-symmetric linkers of equal length, we synthesized a three-helix bundle mimetic that corresponds to the trimeric form of N36.[20] The antisera obtained from mice immunized by the peptide antigen showed strong recognition against the N36 trimer peptide with structural preference. At the same time, the trimer peptide was also investigated as a fusion inhibitor. However, the trimer N36 showed only a threefold increase in inhibition of HIV-1 fusion relative to the N36 monomer.[20] In terms of N36 content, the trimer and monomer have nearly the same inhibitory potency. This phenomenon is consistent with the results from other studies.[21–23] The multimerization of the functional unit, such as synthetic ligands against receptors, show synergistic binding and strong binding activity. Thus, we hypothesized that our strategy using C3-symmetric linkers in the design of trimer mimics of gp41 could be applied to the C34 peptide, which shows significant inhibition potency in the monomeric form. In the present study, we designed and synthesized a novel three-helical bundle structure of the trimeric form of C34. This equivalent mimic of the trimeric form of C34 was evaluated as a novel form of fusion inhibitor.

The C-terminal region of gp41 is known to be an assembly site involving a trimeric coiled-coil conformation. In the design of the C34-derived peptides C34REG-thioester (Figure 1 A) and C34REG (Figure 1 B), the triplet repeat of arginine and glutamic acid (RERERE) was added to the C-terminal end of the C34 sequence (residues 628–661) to increase aqueous solubility, and for C34REG-thioester, a glycine thioester was fused to the C terminus. To form a triple helix corresponding precisely to the gp41 pre-fusion form, we designed the novel C3-symmetric template depicted in Figure 1 C. This designed template linker has three branches of equal length, a hydrophilic structure, and a ligation site for coupling with C34REG-thioester. The template was synthesized as shown in Scheme 1. This approach uses native chemical ligation for chemoselective coupling of unprotected C34REG-thioester with a three-armed cysteine scaffold to produce triC34e (Figure 2).[24,25]

Circular dichroism (CD) spectra of C34REG and triC34e are shown in Figure 3 A. The peptides were dissolved in 50 mM sodium phosphate buffer with 150 mM NaCl, pH 7.2. Both spectra display minima at ~200 nm, indicating that these peptides form random structures. We previously reported that the

[a] Dr. W. Nomura, C. Hashimoto, A. Ohya, Dr. T. Tanaka, Dr. T. Narumi, T. Nakahara, Prof. Dr. H. Tamamura
Institute of Biomaterials and Bioengineering
Tokyo Medical and Dental University
2-3-10 Kandasurugadai, Chiyoda-ku, Tokyo 101-0062 (Japan)
E-mail: tamamura.mr@tmd.ac.jp

[b] Dr. K. Miyauchi, Dr. E. Urano, Dr. J. A. Komano
AIDS Research Center, National Institute of Infectious Diseases
1-23-1 Toyama, Shinjuku-ku, Tokyo 162-8640 (Japan)

[c] Prof. Dr. N. Yamamoto
Department of Microbiology, Yong Loo Lin School of Medicine
National University of Singapore
5 Science Drive 2, Singapore 117597 (Singapore)

Supporting information for this article is available on the WWW under http://dx.doi.org/10.1002/cmdc.201100542.

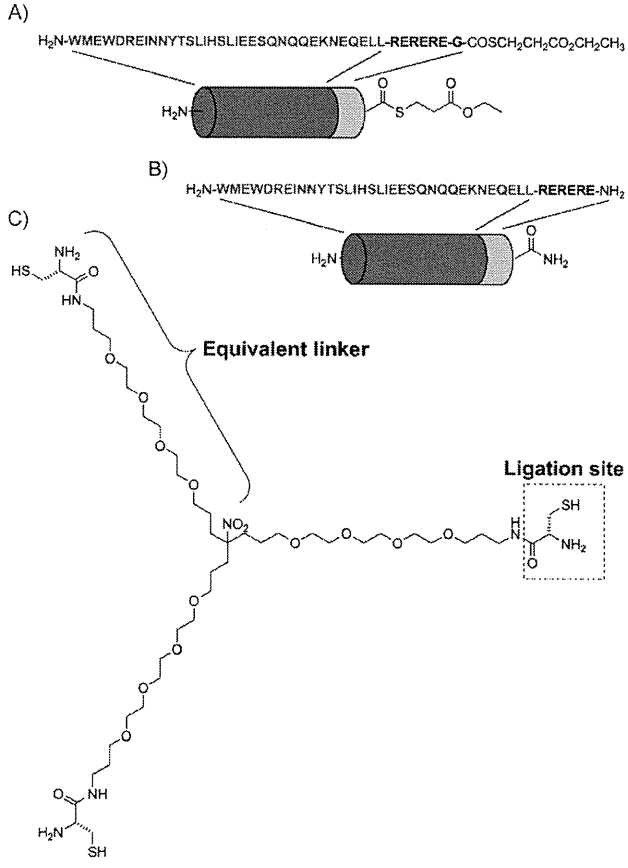

Figure 1. C34-derived peptides: A) C34REG-thioester and B) C34REG. C) The design of a C3-symmetric template.

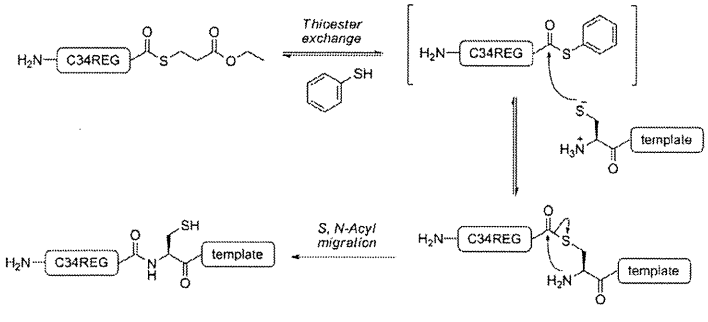

Figure 2. The native chemical ligation used for assembly of the C34REG-thioester on the template.

N36 monomer N36RE and the N36 trimer triN36e form a highly structured α helix, and that the helical content of triN36e was greater than that of N36RE.[20,26] These results suggest that in contrast to N36-derived peptides, C34-derived peptides tend to form random structures both in the monomeric and trimeric forms. To assess the interaction of triC34e with N36, CD spectra of a mixture of triC34e with an N36-derived peptide, N36RE, were measured (Figure 3B). The spectrum of the C34REG and N36RE mixture and that of the triC34e and N36RE mixture showed double minima at λ 208 and 222 nm, indicating that the peptide mixture forms an α-helical structure and that the

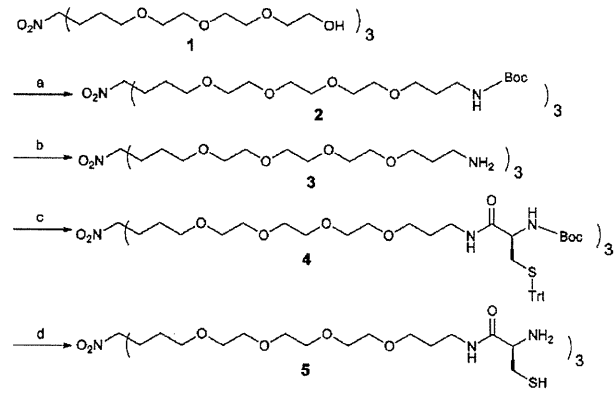

Scheme 1. Synthesis of the equivalently branched template **5**. *Reagents and conditions*: a) (3-bromopropyl)carbamic acid *tert*-butyl ester, NaH, THF; b) 4 M HCl/dioxane; c) Boc-Cys(Trt)-OH, EDCI·HCl, HOBt·H_2O, Et_3N, DMF; d) 90% aq. TFA.

helical content of the trimer triC34e and N36RE mixture is lower than that of the monomer C34REG and N36RE mixture. This is evidence that relative to the monomer C34REG, the trimer triC34e interacts with N36 only with difficulty, due to the assembly of three peptide strands by covalent bonds.

As the trimeric C34 was proven to interact with N36 helices, the potential HIV-1 inhibitory activities of the C-terminal peptides, C34REG and triC34e, were evaluated. The C34 peptide without the solubility-increasing sequence (3×[Arg-Glu], obtained from NIAID) was used as the monomeric control.[27] All peptides showed potent inhibitory activity in the viral fusion assay (Table 1), with the potency of triC34e being 100- and 40-fold higher than that of C34REG and C34 peptides, respectively. Notably, the triC34e trimer peptide is remarkably more potent in anti-HIV-1 activity than the monomer, indicating that a trimeric form is critical for inhibitory activity. Cytotoxicity from the peptides was not observed at concentrations of 15 μM for C34REG and C34, and 5 μM for triC34e.

We next carried out an assay for the inhibition of viral replication. As shown in Table 2, triC34e showed 30- and 20-fold higher inhibitory activity than peptides C34 and C34REG, respectively. In the two anti-HIV-1 assays, triC34e showed a great enhancement of activity over the C34 monomers. The IC_{50} values obtained in the assays are different, and this can be

Table 1. IC_{50} and CC_{50} values determined by viral fusion inhibition and cell viability assays.

	C34 peptide[a]	C34REG	triC34e
IC_{50} [μM][b]	0.044	0.12	0.0013
CC_{50} [μM][c]	>15	>15	>5

[a] HIV-1 IIIB C34 peptide. [b] IC_{50} values are based on luciferase signals in TZM-bl cells infected with HIV-1 (NL4-3 strain). [c] CC_{50} values are based on the decrease in viability of TZM-bl cells. All data are the mean values from at least three experiments.

Table 2. IC_{50} values determined by inhibition assay based on p24 ELISA.			
	C34 peptide	C34REG	triC34e
IC_{50} [μM][a]	1.59	1.06	0.0547
[a] IC_{50} values are based on the production of p24 in MT-4 cells infected with HIV-1 (NL4-3 strain). All data are the mean values from at least three experiments.			

explained through differences in experimental procedures. In the fusion inhibition assay, cells were treated with peptides before viral infection. In contrast, in the viral replication inhibition assay, peptides were treated after viral adsorption to cells. Therefore, in the latter case, the infection by HIV-1 might precede peptide binding to gp41.

It has been shown that T-1249, an analogue of enfuvirtide, and its hydrophobic C-terminal region inhibit HIV-1 fusion by interacting with lipid bilayers.[28] The tryptophan-rich domain of T-1249 was shown to play important roles in HIV-1 fusion.[29–31] As enfuvirtide shows weak interaction with the gp41 core structure, and the C34 sequence lacks the C-terminal lipid binding domain, it has been suggested that C34 has a mechanism of action distinct from that of enfuvirtide.[32] Thus, it is of interest to discern the mechanism of the enhanced inhibition observed with triC34e relative to the monomer. Two explanations can be envisaged: 1) the α helicity of the C34 trimer is higher than that of the monomer, as shown in Figure 3A, and as a result, the C34 trimer binds more strongly to the N36 trimer; and 2) in the mixture with the N36 monomer, the C34 trimer shows less α helicity than its monomer (Figure 3B). As shown in Figure 3A, the molar ellipticity at 222 nm is similar for both the C34 trimer and the monomer. Thus, the decrease at 222 nm in the mixture with N36 might be due to a decrease in the α helicity of N36. These results suggest that the C34 trimer might destabilize helix formation in N36 and thus exert potent inhibitory activity. It has been shown that a dimeric C37 (residues 625–661) variant does not show a significant difference in IC_{50} value against HIV-1 from wild-type C37, although the dimeric peptide shows tighter binding to the gp41 N-HR coiled-coil than the C37 monomer.[33] Thus, the mechanism of action of the C34 trimer could be different from that of the dimeric C-peptide. The detailed action mechanism of the trimer as a fusion inhibitor and the reasons behind its remarkable increased anti-HIV-1 activity will be the subjects of future studies in our research group.

A C-terminal helical peptide of HIV-1 gp41 has been designed as a new HIV fusion inhibitor and was synthesized with a novel template and three branched linkers of equal length. The native chemical ligation proceeded by chemoselective coupling in an aqueous medium of an unprotected C34 derivative containing a C-terminal thioester with a three-cysteine-armed scaffold. This process led to the production of triC34e. As a fusion inhibitor, triC34e has potent anti-HIV-1 activity, 100-fold greater than that of the C34REG monomer, although the anti-HIV-1 activity of the N36 trimer is threefold higher than that of the N36 monomer, and the N36 content is the same in both cases.[20] A trimeric form of C34 is evidently critical as the active structure of the fusion inhibitor. The soluble C34 derivative, SC34, retains potent inhibitory effects against enfuvirtide-resistant viruses,[34] and this suggests that the present highly potent trimeric inhibitor could be effective for enfuvirtide-resistant HIV-1 strains. The design of inhibitors that target the dynamic supramolecular mechanism of HIV-1 fusion will be useful for future studies of anti-HIV-1 agents.

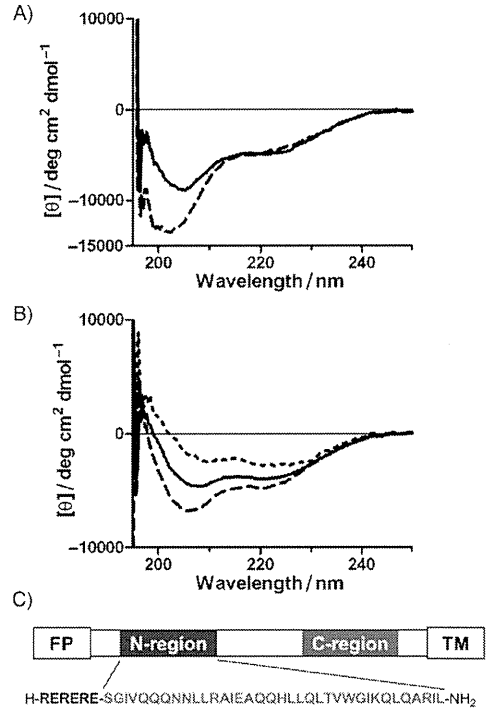

Figure 3. A) CD spectra of C34REG (monomer, -----, 6 μM) and triC34e (trimer, ——, 2 μM). B) CD spectra in the presence or absence of the N36 monomer N36RE:[20] -----, [C34REG (6 μM) + N36RE (6 μM)]; ——, [triC34e (2 μM) + N36RE (6 μM)]; ••••, N36RE (6 μM). In the amino acid sequence of N36RE, the triplet repeat of arginine and glutamic acid is located at the N-terminus of the original N36 sequence.[20] C) Amino acid sequence of N36RE: FP and TM represent the hydrophobic fusion peptide and transmembrane domains, respectively.

Experimental Section

Conjugation of C34REG-thioester and the template to produce triC34e

TCEP·HCl (773 μg, 2.67 μmol) and thiophenol (9 μL, 89 μmol) were dissolved in 0.1 M sodium phosphate buffer (60 μL) containing 6 M urea and EDTA (pH 8.5, 2 mM) under a nitrogen atmosphere. Compound **5** (100 μg, 0.0899 μmol), C34REG-thioester (1.77 mg, 0.297 μmol), and CH_3CN (20 μL) were added. The reaction was stirred for 5 h at 37 °C and monitored by HPLC. The ligation product (triC34e) was separated as an HPLC peak and characterized by ESI-ToF-MS (*m/z* calcd for $C_{703}H_{1108}N_{205}O_{245}S_6$ $[M+H]^+$: 16533.9, found: 16543.8). Purification was performed by reversed-phase HPLC (Cosmosil 5 C_{18}-AR II column, 10×250 mm, Nacalai Tesque, Inc.) with elution using a 33–43% linear gradient of CH_3CN (0.1% TFA) over 40 min. Purified triC34e, obtained in 17% yield, was identified by ESI-ToF-MS. Details of the synthesis of these peptides are described in the Supporting Information.

CD spectra

Circular dichroism measurements were performed with a J-720 CD spectropolarimeter equipped with a thermoregulator (Jasco). The wavelength dependence of molar ellipticity [θ] was monitored at 25 °C from λ 195 to 250 nm. The peptides were dissolved in PBS (50 mM sodium phosphate, 150 mM NaCl, pH 7.2).

Virus preparation

For virus preparation, 293FT cells in a 60 mm dish were transfected with the pNL4-3 construct (10 μg) by the calcium phosphate method. The supernatant was collected 48 h after transfection, passed through a 0.45 μm filter, and stored at −80 °C as the virus stock.

Anti-HIV-1 assay

For the viral fusion inhibition assay, TZM-bl cells (2×10^4 cells per 100 μL) were cultured with the NL4-3 virus (5 ng of p24) and serially diluted peptides. After culture for 48 h, cells were lysed, and the luciferase activity was determined with the Steady-Glo luciferase assay system (Promega, Fitchburg, WI, USA).[35] For the viral replication inhibition assay, MT-4 cells (5×10^4 cells) were exposed to HIV-1 NL4-3 (1 ng of p24) at 4 °C for 30 min. After centrifugation, cells were resuspended with 150 μL medium containing indicated concentrations of serially diluted peptides. Cells were cultured at 37 °C for 3 days, and the concentration of p24 in the culture supernatant was determined by HIV-1 p24 antigen ELISA kit (ZeptoMetrix, Buffalo, NY, USA).

Cytotoxicity assay

The cytotoxic effects of peptides were determined by the CellTiter 96 AQueous One Solution Cell Proliferation assay system (Promega) under the same conditions, but in the absence of viral infection.

Acknowledgements

The following reagent was obtained through the US National Institutes of Health (NIH) AIDS Research and Reference Reagent Program, Division of AIDS, NIAID, NIH: HIV-1 IIIB C34 Peptide from DAIDS, NIAID. This work was supported in part by a Grant-in-Aid for Scientific Research from the Ministry of Education, Culture, Sports, Science, and Technology of Japan, and Health and Labour Sciences Research Grants from the Japanese Ministry of Health, Labor, and Welfare. C.H. is supported by JSPS research fellowships for young scientists.

Keywords: antiviral agents · C34 trimers · fusion inhibitors · gp41 · HIV-1

[1] C. Hashimoto, T. Tanaka, T. Narumi, W. Nomura, H. Tamamura, *Expert Opin. Drug Discovery* **2011**, *6*, 1067–1090.
[2] E. O. Freed, M. A. Martin, *J. Biol. Chem.* **1995**, *270*, 23883–23886.
[3] D. M. Eckert, P. S. Kim, *Annu. Rev. Biochem.* **2001**, *70*, 777–810.
[4] R. Wyatt, J. Sodroski, *Science* **1998**, *280*, 1884–1888.
[5] E. A. Berger, P. M. Murphy, J. M. Farber, *Annu. Rev. Immunol.* **1999**, *17*, 657–700.
[6] M. Lu, S. C. Blacklow, P. S. Kim, *Nat. Struct. Biol.* **1995**, *2*, 1075–1082.
[7] S. Jiang, K. Lin, N. Strick, A. R. Neurath, *Nature* **1993**, *365*, 113.
[8] C. T. Wild, D. C. Shugars, T. K. Greenwell, C. B. McDanal, T. J. Matthews, *Proc. Natl. Acad. Sci. USA* **1994**, *91*, 9770–9774.
[9] C. T. Wild, T. Oas, C. McDanal, D. Bolognesi, T. Matthews, *Proc. Natl. Acad. Sci. USA* **1992**, *89*, 10537–10541.
[10] J. M. Kilby, S. Hopkins, T. M. Venetta, B. DiMassimo, G. A. Cloud, J. Y. Lee, L. Alldredge, E. Hunter, D. Lambert, D. Bolognesi, T. Matthews, M. R. Johnson, M. A. Nowak, G. M. Shaw, M. S. Saag, *Nat. Med.* **1998**, *4*, 1302–1307.
[11] J. M. Kilby, J. J. Eron, *N. Engl. J. Med.* **2003**, *348*, 2228–2238.
[12] J. P. Lalezari, K. Henry, M. O'Hearn, J. S. Montaner, P. J. Piliero, B. Trottier, S. Walmsley, C. Cohen, D. R. Kuritzkes, J. J. Eron, Jr., J. Chung, R. DeMasi, L. Donatacci, C. Drobnes, J. Delehanty, M. Salgo, *N. Engl. J. Med.* **2003**, *348*, 2175–2185.
[13] S. Liu, W. Jing, B. Cheng, H. Lu, J. Sun, X. Yan, J. Niu, J. Farmar, S. Wu, S. Jiang, *J. Biol. Chem.* **2007**, *282*, 9612–9620.
[14] D. C. Chan, D. Fass, J. M. Berger, P. S. Kim, *Cell* **1997**, *89*, 263–273.
[15] E. De Rosny, R. Vassell, R. T. Wingfield, C. T. Wild, C. D. Weiss, *J. Virol.* **2001**, *75*, 8859–8863.
[16] J. P. Tam, Q. Yu, *Org. Lett.* **2002**, *4*, 4167–4170.
[17] W. Xu, J. W. Taylor, *Chem. Biol. Drug Des.* **2007**, *70*, 319–328.
[18] J. M. Louis, I. Nesheiwat, L. Chang, G. M. Clore, C. A. Bewlet, *J. Biol. Chem.* **2003**, *278*, 20278–20285.
[19] E. Bianch, J. G. Joyce, M. D. Miller, A. C. Finnefrock, X. Liang, M. Finotto, P. Ingllinella, P. McKenna, M. Citron, E. Ottinger, R. W. Hepler, R. Hrin, D. Nahas, C. Wu, D. Montefiori, J. W. Shiver, A. Pessi, P. S. Kim, *Proc. Natl. Acad. Sci. USA* **2010**, *107*, 10655–10660.
[20] T. Nakahara, W. Nomura, K. Ohba, A. Ohya, T. Tanaka, C. Hashimoto, T. Narumi, T. Murakami, N. Yamamoto, H. Tamamura, *Bioconjugate Chem.* **2010**, *21*, 709–714.
[21] M. Lu, H. Ji, S. Shen, *J. Virol.* **1999**, *73*, 4433–4438.
[22] D. M. Eckert, P. S. Kim, *Proc. Natl. Acad. Sci. USA* **2001**, *98*, 11187–11192.
[23] E. Bianchi, M. Finotto, P. Ingallinella, R. Hrin, A. V. Carella, X. S. Hous, W. A. Schleif, M. D. Miller, *Proc. Natl. Acad. Sci. USA* **2005**, *102*, 12903–12908.
[24] P. E. Dawson, T. W. Muir, I. Clark-Lewis, S. B. H. Kent, *Science* **1994**, *266*, 776–779.
[25] P. E. Dawson, M. J. Churchill, M. R. Ghadiri, S. B. H. Kent, *J. Am. Chem. Soc.* **1997**, *119*, 4325–4329.
[26] D. C. Chan, C. T. Chutkowski, P. S. Kim, *Proc. Natl. Acad. Sci. USA* **1998**, *95*, 15613–15617.
[27] S. A. Gallo, K. Sackett, S. S. Rawat, Y. Shai, R. Blumenthal, *J. Mol. Biol.* **2004**, *340*, 9–14.
[28] A. S. Veiga, N. C. Santos, L. M. Loura, A. Fedorov, M. A. Castanho, *J. Am. Chem. Soc.* **2004**, *126*, 14758–14763.
[29] M. K. Lawless, S. Barney, K. I. Guthrie, T. B. Bucy, S. R. Petteway, Jr., G. Merutka, *Biochemistry* **1996**, *35*, 13697–13708.
[30] K. Salzwedel, J. T. West, E. Hunter, *J. Virol.* **1999**, *73*, 2469–2480.
[31] S. G. Peisajovich, S. A. Gallo, R. Blumenthal, Y. Shai, *J. Biol. Chem.* **2003**, *278*, 21012–21017.
[32] S. Liu, H. Lu, Y. Xu, S. Wu, S. Jiang, *J. Biol. Chem.* **2005**, *280*, 11259–11273.
[33] K. M. Kahle, K. Steger, M. J. Root, *PLoS Pathog.* **2009**, *5*, e1000674.
[34] A. Otaka, M. Nakamura, D. Nameki, E. Kodama, S. Uchiyama, S. Nakamura, H. Nakano, H. Tamamura, Y. Kobayashi, M. Matsuoka, N. Fujii, *Angew. Chem.* **2002**, *114*, 3061–3064; *Angew. Chem. Int. Ed.* **2002**, *41*, 2937–2940.
[35] E. J. Platt, K. Wehrly, S. E. Kuhmann, B. Chesebro, D. Kabat, *J. Virol.* **1998**, *72*, 2855–2864.

Received: November 22, 2011
Revised: December 15, 2011
Published online on January 13, 2012

AIDS RESEARCH AND HUMAN RETROVIRUSES
Volume 27, Number 00, 2011

DOI: 10.1089/aid.2011.0180

The Hematopoietic Cell-Specific Rho GTPase Inhibitor ARHGDIB/D4GDI Limits HIV Type 1 Replication

Tadashi Watanabe,[1] Emiko Urano,[2] Kosuke Miyauchi,[2] Reiko Ichikawa,[2] Makiko Hamatake,[2] Naoko Misawa,[1] Kei Sato,[1] Hirotaka Ebina,[1] Yoshio Koyanagi,[1] Jun Komano[2]

Abstract

Rho GTPases are able to influence the replication of human immunodeficiency virus type 1 (HIV-1). However, little is known about the regulation of HIV-1 replication by guanine nucleotide dissociation inhibitors (GDIs), one of the three major regulators of the Rho GTPase activation cycle. From a T cell-based cDNA library screening, ARHGDIB/RhoGDIβ, a hematopoietic lineage-specific GDI family protein, was identified as a negative regulator of HIV-1 replication. Up-regulation of ARHGDIB attenuated the replication of HIV-1 in multiple T cell lines. The results showed that (1) a significant portion of RhoA and Rac1, but not Cdc42, exists in the GTP-bound active form under steady-state conditions, (2) ectopic ARHGDIB expression reduced the F-actin content and the active forms of both RhoA and Rac1, and (3) HIV-1 infection was attenuated by either ectopic expression of ARHGDIB or inhibition of the RhoA signal cascade at the HIV-1 Env-dependent early phase of the viral life cycle. This is in good agreement with the previous finding that RhoA and Rac1 promote HIV-1 entry by increasing the efficiency of receptor clustering and virus-cell membrane fusion. In conclusion, the ARHGDIB is a lymphoid-specific intrinsic negative regulator of HIV-1 replication that acts by simultaneously inhibiting RhoA and Rac1 functions.

Introduction

THE HUMAN IMMUNODEFICIENCY VIRUS TYPE I (HIV-1) is the causative agent of acquired immunodeficiency syndrome (AIDS). The clinical success of Maraviroc, an antiretroviral drug that targets the host cell protein CCR5, demonstrates the importance of understanding host-HIV-1 interaction as this information will provide the basis for the development of the next generation of antiretroviral drugs. HIV-1 replicates primarily in CD4-positive T cells. However, aside from the viral receptors CD4 and CCR5, few lymphoid cell-specific regulators of HIV-1 replication have been identified. This is partly due to the use of nonlymphoid cells to screen for cellular factors that regulate HIV-1 replication, as these cells support the efficient transduction of genetic materials. Therefore, T cell-based cDNA library screening has some advantages, as discussed later.

Members of the Rho GTPase family, including RhoA, Rac1, and Cdc42, have been reported to regulate the replication of HIV-1 at various stages of the viral life cycle, including viral entry, transcription, and viral release.[1–7] Although these proteins are widely expressed, genome-wide screens for proteins that regulate HIV-1 replication using siRNA or shRNA libraries have failed to identify Rho GTPases.[8–10] This may suggest that Rho GTPases are not potent regulators of HIV-1 replication and are therefore difficult to detect unless the viral replication assay is employed, since multiple replication cycles augment the biological effects of Rho GTPases.

There are three major regulators of the activation cycle of Rho GTPases: guanine nucleotide exchange factors (GEFs), GTPase-activating proteins (GAPs), and guanine nucleotide dissociation inhibitors (GDIs or ARHGDIs). RhoGEFs promote the exchange of GDP for GTP, RhoGAPs accelerate GTP hydrolysis, and ARHGDIs stabilize the GDI-bound form of Rho GTPases and also mask the lipid moiety of Rho GTPases, thereby sequestering Rho GTPases at the plasma membrane.[11–14] Some RhoGAPs and RhoGEFs have been known to regulate HIV-1 replication.[6,9,10,15–18] Positive regulators of Rho GTPases, such as RhoGEFs, were identified in the genome-wide screens, although these studies yielded varying results. In this sense, the upstream regulators of Rho GTPases may more potently influence HIV-1 replication than Rho GTPases themselves when expression levels are dysregulated. ARHGDIs have yet to be identified as regulators of HIV-1 replication.

[1]Laboratory of Viral Pathogenesis, Institute for Virus Research, Kyoto University, Kyoto, Japan.
[2]AIDS Research Center, National Institute of Infectious Diseases, Tokyo, Japan.

Previously, we established a genetic screening system using a T cell-derived cDNA library to isolate cellular factors that render cells resistant to HIV-1 replication.[19,20] This system is unique in that the screen is based on MT-4 cells, a human CD4-positive T cell line, which were exposed to replication-competent HIV-1. Using this system, the carboxy-terminal domains of Brd4 and SEC14L1a were found to be negative regulators of HIV-1 replication.[19,20] Importantly, these factors were not found in previous genetic screens, suggesting that our system complements other genome-wide analyses. In this study, we describe a lymphoid-specific RhoGDI that negatively regulates HIV-1 replication through attenuation of both RhoA and Rac1 functions.

Materials and Methods

Cells

Cells were maintained in RPMI 1640 medium (Sigma, St. Louis, MO) supplemented with 10% fetal bovine serum (FBS; Japan Bioserum, Tokyo, Japan or Thermo Fisher Scientific Inc., Waltham, MA), 50–100 U/ml penicillin, and 50–100 μg/ml streptomycin (Invitrogen, Tokyo, Japan), and then incubated at 37°C in a humidified 5% CO_2 atmosphere. The selection of cDNA library-transduced cells was described previously.[20] To select puromycin-resistant cells after infection with pQc- or pSM2c-based murine leukemia virus (MLV) vector, 1 μg/ml puromycin (Sigma) was added to the culture medium.

Plasmids

The plasmid vectors pCMMP, pMDgag-pol, pSV-tat, phRL/CMV, and pVSV-G were described previously.[21] The shRNA expression vectors pSM2c and pSM2/ARHGDIB (RHS1764-9680880) were purchased from Thermo Fisher Scientific (Open Biosystems Products, Huntsville, AL). The pQcXIP was obtained from Clontech (BD Biosciences Clontech, Palo Alto, CA). pGEX-Rhotekin-RBD and pGEX-4T-PAK2-RBD were kindly provided by S. Narumiya, Kyoto University.[3,22] To construct pLTR-hRL, the HIV-1_{HXB2} long terminal repeat (LTR) was amplified by PCR using the following primers: 5′-GGA TCC TGG AAG GGC TAA TTC ACT CC-3′ and 5′-GCT AGC TGC AGC TGC TAG AGA TTT TCC ACA CTG-3′. The *BglII-NheI* fragment of the PCR product was cloned into the corresponding restriction sites of phRL/CMV, generating pLTR-hRL. The LTR-Luc plasmid was described previously.[23] To construct pCMV-Tat-FLAG, HIV-1_{NL4-3} *tat* was amplified from cDNA prepared from HIV-1-infected MT-4 cells by RT-PCR using the following primers: 5′-ATG GAG CCA GTA GAT CCT AGA CTA GAG CCC T-3′ and 5′-TTC CTT CGG GCC TGT CGG GT-3′. The PCR product was cloned into the *EcoRV* sites of pcDNA3.1 Zeo(+) bearing FLAG-tags at the *NotI-XhoI* site (Invitrogen). The pCMV-Luc plasmid was a generous gift from Dr. Hijikata (Kyoto University).

Flow cytometry

Cells were incubated with anti-CD4, anti-CD8, or anti-CXCR4 monoclonal antibodies conjugated to R-phycoerythrin (PE; BD Pharmingen, San Diego, CA) for 30 min at 4°C. Cells were washed once with phosphate-buffered saline (PBS) supplemented with 1% FBS and analyzed by FACS Calibur (Beckton Dickinson, San Jose, CA).

Phalloidin staining of F-actin

Phalloidin staining of F-actin was performed as described previously.[24] In brief, cells were fixed, permeabilized by cytofix/cytoperm (BD Bioscience) for 20 min on ice, washed, and stained with Alexa Fluor 647-phalloidin (Invitrogen) for 30 min at 4°C. Samples were kept on ice until analysis by FACS Calibur or Canto II (Beckton Dickinson, San Jose, CA). The flow cytometric data were analyzed using FlowJo version 9.3 (Tree-star Inc., Ashland, OR).

Viruses

The retroviral vector pCMMP, carrying the MT-4 cDNA library and a green fluorescent protein (GFP) expression cassette, was obtained from Takara (Takara, Otsu, Japan). Full-length ARHGDIB was cloned from a lymph node cDNA library (Takara) by RT-PCR using the primers 5′-GCA CCG GTC TCG AGC CAC CAT GAC TGA AAA AGC CCC AGA GC-3′ and 5′-CCA ATT GGA TCC TCA TTC TGT CCA CTC CTT CTT AAT CG-3′, and cloned into the pCMMP vector. The MLV vectors were produced by tripartite transfection of pMDgag-pol, pVSV-G, and either pCMMP, pQc, or pSM2c retroviral vector. Cells were infected with the MLV vectors as described previously.[21] The production of replication-competent HIV-1_{HXB2} and the measurement of replication kinetics were performed as described previously.[21]

Western blotting

Western blotting was performed according to techniques described previously.[25] The following monoclonal antibodies were used: anti-RhoA (C-11; Santa Cruz Biotechnology, Santa Cruz, CA), anti-Rac1 (23A8; Millipore, Japan), anti-Cdc42 (B-8; Santa Cruz Biotechnology), anti-ARHGDIB (A01; Abnoba, Taiwan), anti-$p24^{CA}$ (183-H12-5C; NIH AIDS Research and Reference Reagent Program), anti-actin (clone C4; Millipore), and anti-tubulin (DM1A; Sigma). Densitometric analysis was performed using ImageJ ver. 1.43 software (obtained from http://rsbweb.nih.gov/ij/index.html).

Active Rho GTPase capture assay

We adopted a protocol described previously.[3,22] In brief, the glutathione *S*-transferase (GST) fused to the Rho GTPase binding domain (RBD) of Rhotekin and GST fused to the RBD of PAK2 were expressed in *E. coli* and purified by incubating the cell lysates with glutathione-Sepharose 4B beads (GE Healthcare Bio-Sciences, Piscataway, NJ) for 3 h at 4°C. The beads were washed three times with ice-cold Rho buffer (25 mM HEPES, pH 7.5, 150 mM NaCl, 10 mM $MgCl_2$, 1 mM EDTA, 10% Glycerol). Finally, the beads were washed with ice-cold Rho buffer supplemented with 1% NP-40 and protease inhibitor cocktail tablets (Complete, Roche Diagnostics GmbH, Mannheim, Germany). Cells were incubated in ice-cold Rho buffer for 15 min on ice, and the cell lysates were clarified by centrifugation at 18,000 × *g* at 4°C for 20 min. A fraction of the cleared cell lysates was incubated at 37°C for 30 min as a negative control or coincubated with GTPγS (0.1 mM, Sigma) for 30 min at 30°C as a positive control. These preparations were incubated with the above beads at 4°C for 1 h. The beads were washed three times with Rho buffer containing 1% NP-40 and subjected to SDS-PAGE followed by Western blotting. The bead-bound GTPases were detected

using a monoclonal antibody against RhoA, Rac1, or Cdc42, as appropriate.

Single-round infection assay

Single-round virus infection and luciferase assays were performed as described previously.[21,26] In brief, cells were exposed to viral preparations containing 1–10 ng of $p24^{CA}$. Luciferase activities were measured at 2–3 days postinfection with the Picagene luciferase assay kit (Toyo Ink, Tokyo, Japan) or Steady-Glo kit (Promega, Tokyo, Japan) according to the manufacturer's protocols. For the inhibition of Rho-kinase (ROCK), cells were pretreated with 12.5 μM Y27632 (Nakalai tesque, Kyoto, Japan) for 1 h and incubated with the viral preparation in the presence of 12.5 μM Y27632 for 4 h. Cells were washed with tissue culture medium and cultivated for 2 days. Light emission was detected with a 1420 ARVOSX multilabel counter (Perkin Elmer, Wellesley, MA) or a Veritas luminometer (Promega).

Single-round production assay

Five million PM1/control or PM1/ARHGDIB cells were resuspended in 250 μl of STBS (25 mM Tris-Cl, pH 7.4, 137 mM NaCl, 5 mM KCl, 0.6 mM Na_2HPO_4, 0.7 mM $CaCl_2$, and 0.5 mM $MgCl_2$), including 10 μg of pHXB2 proviral plasmid DNA. Cells were mixed with 250 μl of STBS containing 1 mg/ml of DEAE-Dextran and incubated for 30 min at room temperature (RT). The cells were then incubated with STBS containing 10% DMSO for 2 min at RT and washed with 1 ml HBSS (Invitrogen). Transfected cells were cultured in RPMI medium containing 10% FBS and 1 μM efavirenz. After 2 days in culture, viruses in the culture supernatant were pelleted by ultracentrifugation on a 20% sucrose cushion. Cells and viruses were lysed with radioimmunoprecipitation assay (RIPA) lysis buffer (0.05 M Tris-HCl, 0.15 M NaCl, 1% Triton X-100, 0.1% sodium dodecyl sulfate, and 1% sodium deoxycholate) and electrophoresed in a 10% polyacrylamide gel for SDS–PAGE. Proteins were then transferred to a PVDF membrane, and $p24^{CA}$ was detected by immunoblot analysis using an anti-$p24^{CA}$ antibody.

Reporter expression assay

The luciferase-expressing reporter plasmids were transfected into PM1 cells according to the DEAE-Dextran method as described above. For transfection, either 1 μg of pCMV-Luc, 10 μg of pLTR-Luc, 0.5 μg of phRL/CMV, or 1 μg of pLTR-hRL was used. The pLTR-Luc and pLTR-hRL were co-transfected with 5 μg of pCMV-tat-FLAG and 1 μg of pSVtat, respectively. Firefly luciferase activity was measured as described above. Renilla luciferase activity was also measured as described above, except that the Renilla Luciferase Assay System (Promega) was used in place of the Steady-Glo kit. The data were analyzed using a two-tailed Student's *t*-test.

Results

Identification of RhoGDIβ/ARHGDIB as a negative regulator of HIV-1 replication

A pool of MT-4 cells constitutively expressing a cDNA library transduced with an MLV-based retroviral vector was used to screen for possible regulators of HIV-1 replication. The MLV vector carried an expression cassette for GFP and inserts from a cDNA library derived from MT-4 cells (Fig. 1A). The cDNA-transduced cells were enriched with a cell sorter using GFP as a marker. These cells were then infected with CXCR4-using (X4) $HIV\text{-}1_{HXB2}$. MT-4 cells have been shown to support efficient HIV-1 production and rapidly undergo cell death after infection. The surviving MT-4 cells were propagated and genomic DNA was isolated to identify the inserted cDNA, as described previously.[19] These genes were considered potential negative regulators of HIV-1 replication. A cDNA clone encoding ARHGDIB (RhoGDIβ/LyGDI/D4GDI; gene ID 397) was recovered from the MT-4 cDNA library (1/94 independent clones, 1.1%).

Full-length ARHGDIB cDNA was cloned into the MLV vector pQcXIP, and a T cell line expressing ARHGDIB at levels higher than endogenous levels was established. To verify the HIV-1-resistant phenotype of ARHGDIB, the rate of HIV-1 replication was assessed in MT-4 cells subjected to ectopic ARHGDIB expression. In these cells, ARHGDIB levels were increased by approximately 4.9-fold compared with control cells, while the cell surface expression of CD4 and CXCR4 was not significantly affected in MT-4 cells (Fig. 1B). Even the modest up-regulation of ARHGDIB delayed HIV-1 replication kinetics (Fig. 1B). Suppression of HIV-1 replication was independently reproduced in MT-4 cells, even when a different retroviral vector, pCMMP, was used to transduce ARHGDIB (data not shown). In addition, neither the rate of cell proliferation nor cell morphology was affected by stable ectopic expression of ARHGDIB over at least 6 months in culture (data not shown). Delayed HIV-1 replication in cells ectopically overexpressing ARHGDIB was also observed in PM1 (Fig. 1C), M8166 (Fig. 1D), and Jurkat cells (Fig. 1E), in which ARHGDIB levels were increased by 2.1-, 1.9-, and 1.5-fold, respectively, compared with control levels. Similar data were also obtained in SUP-T1 cells (data not shown). The delayed HIV-1 replication in cells ectopically expressing ARHGDIB was reproduced in 10 independent experiments ($p < 0.01$, two-sided binomial test), strongly suggesting that ARHGDIB attenuates the replication of HIV-1. These results indicate that enhanced expression of ARHGDIB renders cells resistant to HIV-1 replication. Consistent with these data, the shRNA-mediated down-regulation of ARHGDIB accelerated the replication of HIV-1 in MT-4 cells (Fig. 1F). These data support the idea that ARHGDIB is a negative regulator of HIV-1 replication.

The RhoGDI family has three members, α, β, and γ, which correspond to ARHGDI A, B, and C, respectively.[11] RhoGDI family members are known to regulate Rho GTPases, including RhoA, Rac1, and Cdc42, although some nonredundant functions of RhoGDIs have been reported.[27] ARHGDIB/RhoGDIβ is primarily expressed in cells of a hematopoietic lineage. Given that Rho GTPases are known to be positive regulators of HIV-1 replication and that ARHGDIB is a negative regulator of Rho GTPases in hematopoietic cells, the function of ARHGDIB was investigated in further detail.

Molecular mediators in the inhibition of HIV-1 replication by ARHGDIB

Under *in vitro* culture conditions, T cell lines show a constitutively activated cell phenotype, and Rho GTPases, including RhoA, Rac1, and Cdc42, have been implicated in T cell

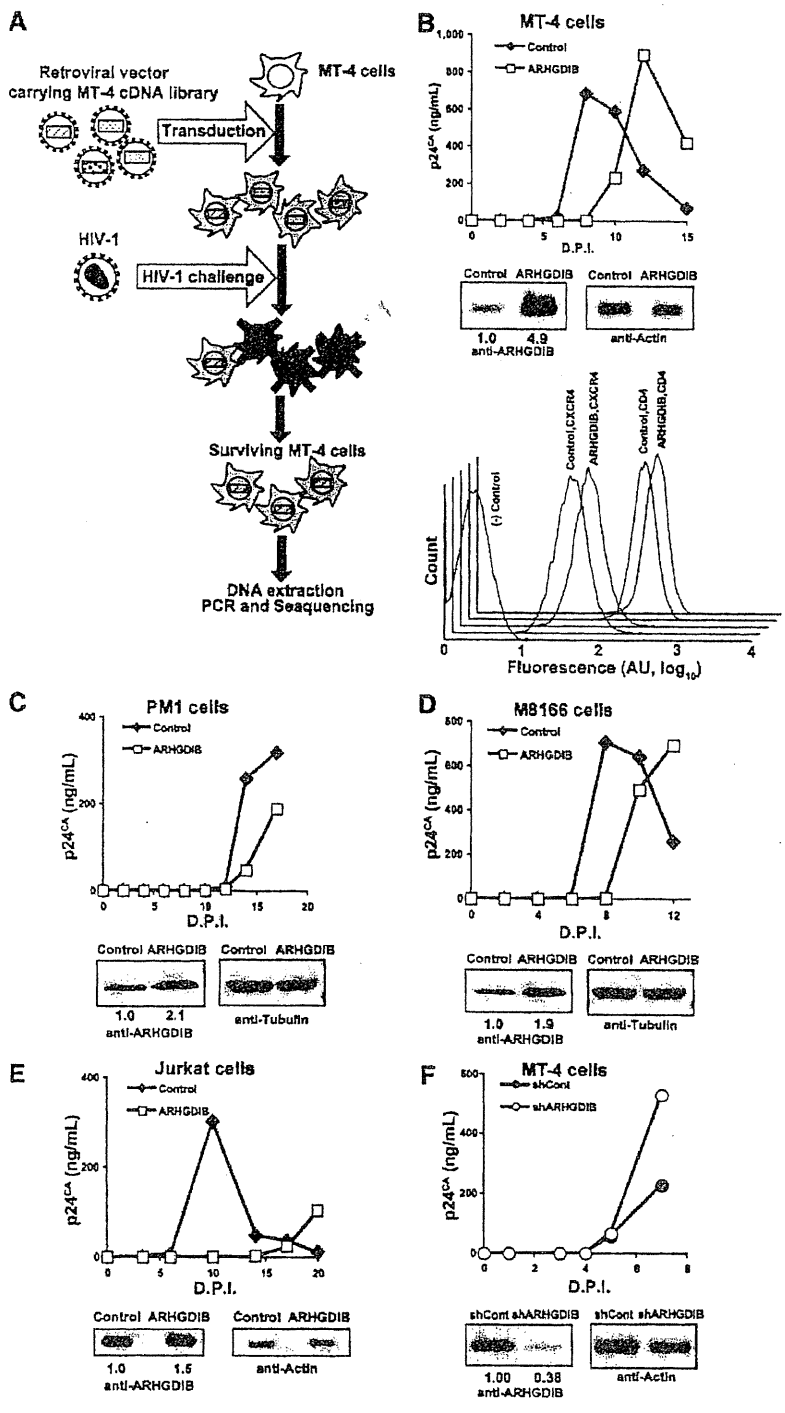

FIG. 1. Isolation and characterization of ARHGDIB as a negative regulator of HIV-1 replication. (A) The screening strategy used to isolate genes that render MT-4 cells resistant to HIV-1 replication. (B–E) Ectopic expression of ARHGDIB (open rectangles) in MT-4 (B), PM1 (C), M8166 (D), and Jurkat (E) cells delayed the replication kinetics of HIV-1. Representative data from five, two, and two independent experiments for MT-4, M8166, and Jurkat cells are shown, respectively. The control counterpart is shown as filled diamonds. (B) The flow cytometric profiles of MT-4 cell surface CD4 and CXCR4 are shown. MT-4/ARHGDIB cells stained for CD8 were used as a negative control. (F) Down-regulation of ARHGDIB (open circles) in MT-4 cells accelerated the replication of HIV-1. The control counterpart is shown as filled circles. (B–F) Expression levels of ARHGDIB and an internal control, either actin or tubulin, were assessed by Western blot analysis. The magnitude of ARHGDIB up- or down-regulation was determined by densitometry and is indicated below each image. AU, arbitrary unit; D.P.I., days postinfection.

activation.[28–30] These Rho GTPases are expressed in various T cell lines, including MT-4, PM1, and M8166 cells, as confirmed by RT-PCR analysis (data not shown). It seemed likely that augmented ARHGDIB expression affected HIV-1 replication by modulating the activity of these Rho GTPases. Thus, the activation status of RhoA, Rac1, and Cdc42 was determined in relation to the enhanced expression of ARHGDIB.

Rho GTPases are intrinsically inefficient hydrolyzing enzymes that quickly cycle between GTP-bound active and GDP-bound inactive forms. If ARHGDIB attenuates HIV-1 replication by inhibiting Rho GTPase activities, some fraction of Rho GTPases would exist in a GTP-bound active form under steady-state tissue culture conditions, and this population should be decreased in cells ectopically expressing ARHGDIB. Using an active Rho GTPase capture assay, the levels of active Rho GTPases in control and ARHGDIB-expressing cells were measured (Fig. 2A). In this assay, GTP-bound Rho GTPase is captured by glutathione-Sepharose beads conjugated to GST fused to the Rho binding domain of Rhotekin or PAK2. The active forms of both RhoA and Rac1, but very little Cdc42, were detected in PM1 cells under steady-state tissue culture conditions (Fig. 2B–D). Activation levels under the steady-state conditions were estimated by comparing the captured Rho GTPase signals with the maximal activation levels, which were established by converting all Rho GTPases to an active form by GTPγS before the pull-down procedure. The activated fractions of Rac1, RhoA, and Cdc42 were 34.2%, 23.2%, and 0.0%, respectively (Fig. 2B–D). Importantly, ectopic expression of ARHGDIB reduced the activated fractions of RhoA and Rac1 to 4.1% and 3.6%, respectively (Fig. 2B and C). Similar observations were made for MT-4 and SUP-T1 cells (data not shown).

These observations clearly indicated that ARHGDIB attenuates RhoA and Rac1 activity simultaneously in these T cell lines and suggested that RhoA and Rac1 are the primary targets of ectopically expressed ARHGDIB. Note that RhoA and Rac1 levels were increased by 1.4- and 1.3-fold, respectively, in cells ectopically expressing ARHGDIB, according to the densitometric analysis (Fig. 2B and C). This is due to the ARHGDIB-mediated stabilization of Rho GTPases, as

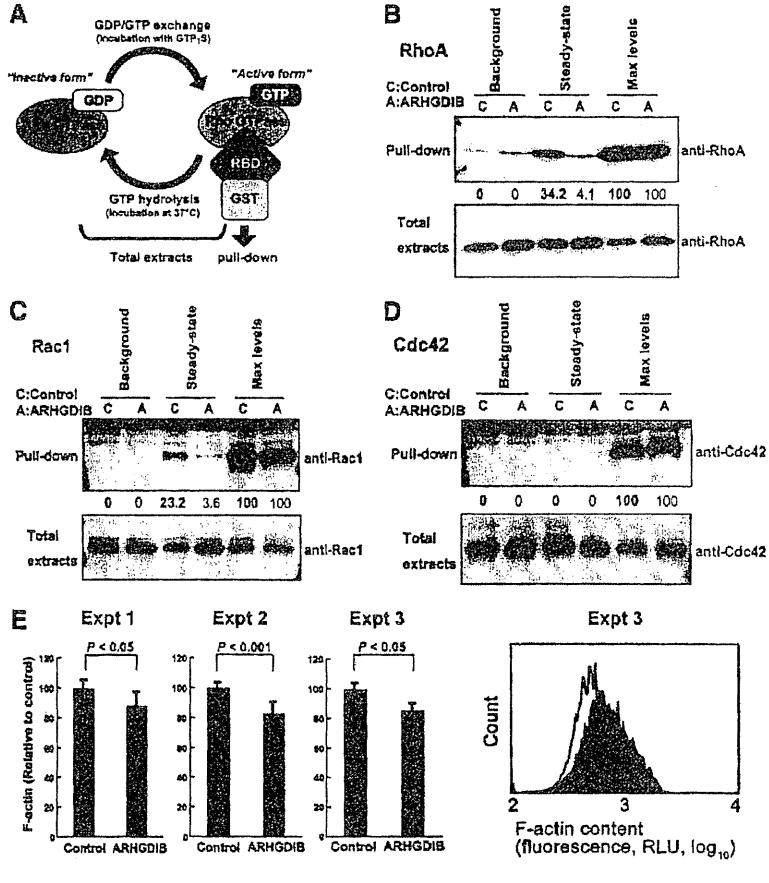

FIG. 2. Activation of RhoA and Rac1 under steady-state conditions in PM1 cells. (A) The experimental procedure for the active Rho GTPase capture assay. The active GTP-bound form is collected by glutathione-Sepharose beads coated with an RBD-GST fusion protein and compared with the total expression levels of each Rho GTPase by Western blot analysis. Incubation of the cell lysate with GTPγS shifts the equilibrium to the right, and incubation of the cell lysate at 37°C for 30 min shifts it to the left, representing the maximal activation levels (Max levels in B–D) or the background levels (background in B–D) of each Rho GTPase, respectively. (B–D) Activation of RhoA (B), Rac1 (C), and Cdc42 (D) in PM1 cells. The activation levels under steady-state conditions were estimated by densitometric analysis defined by setting the Max levels and background to 100% and 0%, respectively. (E) Measurement of F-actin content in PM1/ARHGDIB and control cells. Data from three independent experiments are shown in the bar graphs, and each of these experiments was performed in triplicate. The right panel shows the flow cytometric profile of Experiment 3, in which PM1/ARHGDIB is indicated by a black line, and the control is shown in gray. Statistical significance between the two groups was analyzed by two-tailed Student's *t*-test. AU, arbitrary unit.